Supporting Information

C_{sp2}-H/F bond activation and borylation with low valent iron

Ethan Zars,[a] Lisa Pick,[b] Achala Kankanamge,[a] Michael Gau,[a] Karsten Meyer,[b]* and Daniel. J. Mindiola[b]*

[a]*Department of Chemistry, University of Pennsylvania, 231 S 34th St, Philadelphia, PA, USA 19104*

[b]*Department of Chemistry & Pharmacy, Inorganic Chemistry, Friedrich-Alexander-Universität Erlangen - Nürnberg (FAU) 91058 Erlangen, Germany*

**Corresponding Authors: Karsten Meyer, email: karsten.meyer@fau.de and Daniel J. Mindiola, email: mindiola@sas.upenn.edu*

1 Contents

Material and Methods

2.1 General Considerations. All air sensitive manipulations were carried out in an MBraun Labmaster glovebox or using standard high vacuum Schlenk techniques under an N_2 atmosphere unless otherwise stated. Solvents were purchased from Fisher Scientific, sparged with argon gas for 20 minutes, and dried by passing through two columns of Q5 Alumina and transferred to the glovebox in thick-walled reaction vessels. All solvents were stored over 4Å molecular sieves and sodium chunks inside the glovebox. Molecular sieves, alumina, and celite were activated by heating to 250 °C under dynamic vacuum overnight. Deuterated benzene and tetrahydrofuran (thf) were purchased from Cambridge Isotope Laboratories, dried over a potassium mirror overnight, degassed, and vacuum transferred into a 100 mL Schlenk tube before being brought into the glovebox for use. $^{t\text{Bu}}$pyrr$_2$pyrH$_2$,[1] [Fe{N(SiMe$_3$)$_2$}$_2$],[2] [($^{t\text{Bu}}$pyrr$_2$pyr)Fe(OEt$_2$)],[3] [K$_2${($^{t\text{Bu}}$pyrr$_2$pyr)Fe}$_2$(μ-N$_2$)],[4] and [{K$_2$(18-C-6)($^{t\text{Bu}}$pyrr$_2$pyr)Fe}$_2$(μ-N$_2$)][4] were synthesized according to literature procedures. 18-crown-6 was purchased from TCI Organics and crystallized from acetonitrile before being dried under vacuum overnight. Potassium graphite (KC_8) was prepared by heating equimolar amounts of potassium metal and graphite at 120 °C for two hours until all potassium metal was reacted away. All other chemicals were purchased from commercial sources and used without further purification. All glassware was rigorously cleaned and stored in a 120 °C oven for at least one day before being brought into the glovebox under overnight vacuum. All NMR spectral data were collected on a Bruker AVII-500 MHz, or Bruker Uni-400 MHz instrument. NMR chemical shifts were referenced to the corresponding solvent residual signal (7.16 ppm for ^{1}H NMR), trifluoroborane diethyl ether adduct (BF_3-OEt_2) for ^{11}B, and tetramethylsilane (Me_4Si) for ^{29}Si NMR. Solution state magnetic moments were calculated using Evans Method.[5] Diamagnetic corrections were applied using Pascal's constants.[6] *Safety Note: KC_8 is a strong reductant and pyrophore which can react violently with oxygen and water. KC_8 should only be handled under an inert atmosphere and quenched with a benzoic acid solution before disposal.*

2.2 Zero-field ^{57}Fe-Mössbauer Information. Zero-field ^{57}Fe-Mössbauer spectra were recorded on a WissEl Mössbauer spectrometer (MRG-500) at a temperature of 77 K in constant acceleration mode. ^{57}Co/Rh was used as -radiation source. WinNormos for Igor Pro software was used for the quantitative evaluation of the spectral parameters (least squares fitting to Lorentzian peaks). The minimum experimental line widths were 0.21 mm s^{-1} (full width at half maximum, FWHM). The temperature of the sample was controlled by a MBBC-HE0106 MÖSSBAUER He/N2 cryostat within an accuracy of +/–0.3 K. Least-square fitting of the Lorentzian signals was carried out with the "Mfit" software, developed by Dr. Eckhard Bill (MPI CEC, Mülheim/Ruhr).[7] The isomer shifts were reported relative to α-iron reference at 300 K.

2.3 Magnetism Measurements. Magnetism data of microcrystalline and powdered samples (21.0–25.0 mg), loaded within a polycarbonate gel capsule loaded and compressed into a quartz glass holder, were collected on a Quantum Design MPMS-3 SQUID magnetometer. The DC moment was recorded in the temperature range of 2–300 K with an applied DC field of 1 T, if not stated otherwise. The DC moment was converted into molar magnetic susceptibility (χ_M) using the following formula (with H = magnetic field, n = moles of substance):

χ_M=(DC moment)/(H·n)

Values of the magnetic susceptibility were corrected for core diamagnetism (χ_{dia}) of the sample using tabulated Pascal's constants.[6] Effective magnetic moments (μ_{eff}) were calculated using the following formula (with temperature (T)):

$\mu_{eff}=2.828\cdot((\chi_M-\chi_{dia})T)^{1/2}$

For simulation and analysis of the data, the program "JulX2", written by Dr. Eckhard Bill (MPI CEC, Mülheim/Ruhr) was used.[8]

3 Experimental Procedures

3.1 Preparation of [{K(18-crown-6)}$_2$($^{t\text{Bu}}$pyrr$_2$pyr)Fe(N$_2$)] (2). In a 20 mL scintillation vial 54.1 mg [K$_2${($^{t\text{Bu}}$pyrr$_2$pyr)Fe}$_2$(μ-N$_2$)] (**1**, 0.05 mmol) was dissolved with a magnetic stir bar in 10 mL toluene. In a 4 mL scintillation vial 52.8 mg 18-crown-6 (0.2 mmol) was dissolved in 2 mL toluene. This 18-crown-6 solution was added to a 4 mL scintillation vial containing 21.4 mg KC_8 (0.15 mmol). The 18-crown-6 vial was rinsed with one pipette toluene and the washings were added to the KC_8 vial. The combined KC_8/18-crown-6 suspension was added to the toluene solution of **1** dropwise at room temperature while stirring. The KC_8/18-crown-6 vial was rinsed with one pipette toluene and the washings added to the reaction mixture. A brown oil initially formed along with a slight color change from dark brown to dark yellow/green. The reaction mixture was stirred for one hour at room temperature after which the brown oil disappeared and the solution color changed to dark purple. The reaction mixture was filtered through a pad of celite and concentrated to 1 mL before being placed in a -35 °C freezer to crystallize overnight. The supernatant was decanted, and the black crystalline material redissolved in 1 mL toluene and placed in a -35 °C freezer for a second crystallization. The supernatant was decanted, and the black crystalline material dried under vacuum. Single crystals suitable for X-Ray diffraction studies were grown by slow evaporation of a diethyl ether solution of **2** at room temperature. Yield: 45.1 mg (0.04 mmol, 79.2%). **^{1}H NMR**, (C_6D_6, 500 MHz, 298 K) δ = 50.83 ($\nu_{1/2}$ = 50.5 Hz), 31.49 ($\nu_{1/2}$ = 82.4 Hz), 7.47 ($\nu_{1/2}$ = 30.6 Hz), 4.29 ($\nu_{1/2}$ = 20.0 Hz), 3.86 ($\nu_{1/2}$ = 200.0 Hz), 1.82 ($\nu_{1/2}$ = 30.6 Hz), -2.52 ($\nu_{1/2}$ = 149.7 Hz). **Magnetic Moment**, (Evans Method, C_6D_6, 500 MHz, 298 K): μ_{eff} = 4.1 μ_B (S = 2). **IR**, (solid, KBr pellet, cm^{-1}): 3090 (w), 2893 (br), 1942 (w), 1851 (s, $\underline{N_2}$), 1539 (w), 1451 (s), 1351 (s), 1250 (s), 1105 (s), 962 (s), 838 (w).

3.2 Preparation of [{K(18-crown-6)}($^{t\text{Bu}}$pyrr$_2$pyr)Fe(C$_6$H$_5$)] (3). In a 20 mL scintillation vial 57.5 mg [{K(18-crown-6)}$_2$($^{t\text{Bu}}$pyrr$_2$pyr)Fe(N$_2$)] (**2**, 0.05 mmol) was dissolved in 1 mL benzene. In a 4 mL scintillation vial 11.6 mg bispinacolato diboron (B_2Pin_2, 0.05 mmol) was dissolved in 0.5 mL benzene and added to the benzene solution of **2**. The vial was sealed with electrical tape and left at room temperature for 16 hours after which time the solution turned from dark

purple/black to red and a crystalline red solid deposited on the vial floor. The supernatant was decanted and the red crystalline solid washed three times with 2 mL pentane and dried under vacuum. **Yield:** 28.8 mg (0.03 mmol, 61.2%). Crystalline material obtained in this fashion was suitable for X-Ray diffraction studies. **^{1}H NMR**, (thf-d_8, 500 MHz, 298 K) δ = 121.08 ($\nu_{1/2}$ = 185.4 Hz, pyrr/pyr*H*-2H), 86.87 ($\nu_{1/2}$ = 32.3 Hz, C_6H_5-3H), 72.11 ($\nu_{1/2}$ = 132.0 Hz, pyrr/pyr*H*-2H), 16.66 ($\nu_{1/2}$ = 75.5 Hz, C_6H_5-2H), 5.05 ($\nu_{1/2}$ = 21.7 Hz, pyrpyrr$_2$^{t}Bu*H*-18H), 2.00 ($\nu_{1/2}$ = 56.8 Hz, 18-crown-6*H*-24H), -4.07 ($\nu_{1/2}$ = 497.4 Hz, pyrpyrr$_2$^{t}Bu*H*-18H), -8.94 ($\nu_{1/2}$ = 38.4 Hz, pyr*H*-1H). **Magnetic Moment**, (Evans Method, thf-d_8, 500 MHz, 298 K): μ_{eff} = 4.8 μ_B (S = 2). **UV-Vis**, tetrahydrofuran [nm (max/sh, $M^{-1}\cdot cm^{-1}$)]: 346 (max, 19600), 429 (max, 8060), 530 (sh, 113).

3.3 Preparation of [{K(18-C-6)(thf)$_2$}($^{t\mathrm{Bu}}$pyrr$_2$pyr)FeCl] (5). In a 20 mL scintillation vial 54.1 mg [K$_2${($^{t\mathrm{Bu}}$pyrr$_2$pyr)Fe}$_2$(μ-N$_2$)] (**1**, 0.05 mmol) was dissolved in 10 mL toluene. In a 4 mL scintillation vial 26.4 mg 18-crown-6 (0.1 mmol) was dissolved in 2 mL toluene. To the 18-crown-6 solution 7.5 μL trimethylsilylchloride (Me$_3$SiCl, 0.1 mmol) was added via microsyringe. The combined 18-crown-6/Me$_3$SiCl solution was added to the solution of **1** dropwise while stirring at room temperature. The 18-crown-6/Me$_3$SiCl vial was rinsed with 2 mL toluene and the washings were added to the reaction mixture. The reaction mixture was stirred for 16 hours at room temperature. An initial formation of a brown oil was observed followed by a slow color change of the solution from dark brown/black to red. The solvent was evacuated and the resulting solid dissolved in 0.5 mL thf. The thf solution was placed in a -35 °C freezer overnight after which time red crystals formed on the vial floor. The supernatant was decanted and the crystals dried under vacuum. **Yield:** 44.9 mg (0.46 mmol, 92%). Crystalline material obtained in this fashion was suitable for X-Ray diffraction studies. **^{1}H NMR**, (thf-d_8, 500 MHz, 298 K) δ = 113.76 ($\nu_{1/2}$ = 144.2 Hz, pyrr/pyr*H*-2H), 98.53 ($\nu_{1/2}$ = 33.7 Hz, pyrr/pyr*H*-2H), 18.66 ($\nu_{1/2}$ = 35.2 Hz, pyr*H*-1H), 7.28 ($\nu_{1/2}$ = 23.0 Hz, pyrpyrr$_2$^{t}Bu*H*-18H), -1.87 ($\nu_{1/2}$ = 81.0 Hz, pyrpyrr$_2$^{t}Bu*H*-18H+18-crown-6*H*-24H). **Magnetic Moment**, (Evans Method, thf-d_8, 500 MHz, 298 K): μ_{eff} = 5.4 μ_B (S = 2). **UV-Vis**, tetrahydrofuran [nm (max/sh, $M^{-1}\cdot cm^{-1}$)]: 343 (max, 27200), 430 (max, 11300), 538 (sh, 1210).

3.4 Formation of [{K(18-crown-6)}HB_2Pin_2] (4). The supernatant from the preparation of **3** was evacuated to dryness and the resulting white/orange solid dissolved in 0.5 mL thf. The thf solution was layered with pentane and placed in a -35 °C freezer overnight to crystallize. Off-white crystals formed and could be structurally characterized by single crystal X-Ray diffraction studies. This crystalline material was also analyzed by ^{11}B NMR spectroscopy, and two resonances were observed at 31.0 and 5.9 ppm consistent with one trigonal B atom and one tetrahedral B atom. These same resonances were observed in the ^{11}B NMR spectrum of the crude supernatant of **3** albeit at slightly different chemical shift values, likely due to paramagnetic effects from the presence of small amounts of **3** in the supernatant.

3.5 Reaction of [{K(18-crown-6)}$_2$($^{t\text{Bu}}$pyrr$_2$pyr)Fe(N_2)] with two eq. 18-crown-6. In 4 mL scintillation vial, 8.5 mg [{K(18-crown-6)}$_2$($^{t\text{Bu}}$pyrr$_2$pyr)Fe(N_2)] (0.005 mmol) was dissolved in approximately 0.5 mL C_6D_6 and pipetted into a J. Young NMR tube. An initial ^{1}H NMR spectrum was recorded. The NMR tube was returned to the glovebox and a C_6D_6 solution of 2.6 mg 18-crown-6 (0.01 mmol) was added. No immediate color change could be observed. A ^{1}H NMR spectrum was recorded approximately 30 minutes after addition of the 18-crown-6 and disappearance of the resonances attributable to [{K(18-crown-6)}$_2$($^{t\text{Bu}}$pyrr$_2$pyr)Fe(N_2)] could be observed. The NMR tube was left at room temperature for one day after which the solution color turned red and some solid material precipitated out of solution. ^{1}H NMR spectroscopy showed only a few indistinct resonances that could not be assigned to any known molecules, indicating decomposition of the iron containing molecules.

3.6 Reaction of 1 with two eq. Me_3SiCl and 18-crown-6. In a 4 mL scintillation vial, 10.8 mg **1** (0.1 mmol) was dissolved in approximately 0.5 mL C_6D_6, pipetted into a J. Young NMR tube, and an initial ^{1}H NMR spectrum was taken. The NMR tube was returned to the glovebox. In a 4 mL scintillation vial 5.3 mg 18-crown-6 (0.2 mmol) was dissolved in minimal C_6D_6. To this solution, 1.5 μL trimethylsilylchloride (0.2 mmol, Me_3SiCl) was added via microsyringe. The combined 18-crown-6/Me_3SiCl solution was added to the NMR tube and the NMR tube was inverted a few times to ensure proper mixing of reagents. A brown oil was observed to form

initially. A ^{1}H NMR spectrum was taken approximately 30 minutes after mixing of reagents. The NMR tube was left to stand at room temperature overnight after which time the brown oil disappeared and the solution turned dark red. A ^{1}H NMR spectrum showed formation of **5** along with an unknown impurity. A ^{29}Si INEPT spectrum showed a resonance at 7.19 ppm attributable to the ether hexamethyl disiloxane (HMDSO).[9] The formation of HMDSO is likely due to rapid decomposition of a reactive initial product of Me_3SiCl reduction.

3.7 Formation of 3 from reaction of 2 with fluorobenzene. In a 20 mL scintillation vial, 10.5 mg **2** (0.0092 mmol) was dissolved in 0.5 mL fluorobenzene. The black compound immediately formed a red solution. The solution was placed in the freezer overnight to crystallize. Light red crystals formed overnight and were collected by decanting the supernatant and drying the crystals under vacuum. The mass of the crystalline material was too small to be measured but a ^{1}H NMR spectrum of this material could be recorded in thf with a thf-d_8 capillary and shows a mixture of **3** and another unidentified paramagnetic compound. The supernatant was evacuated and dissolved in thf with a thf-d_8 capillary. A ^{1}H NMR spectrum of the supernatant shows the same paramagnetic resonances as the crystalline material and the ^{19}F NMR spectrum shows only a single resonance at -113.5 ppm indicative of residual fluorobenzene.[10]

3.8 Reaction of 2 with *N*-Benzylidene benzylamine. In a 4 mL scintillation vial, 11.7 mg **2** (0.1 mmol) was dissolved in approximately 0.5 mL C_6D_6 and pipetted into a J. Young NMR tube. An initial ^{1}H NMR spectrum was recorded. The NMR tube was returned to the glovebox and 2 uL neat *N*-Benzylidene benzylamine (0.1 mmol) was added to the NMR tube via microsyringe. The NMR tube was inverted a few times to ensure proper mixing of reagents. A ^{1}H NMR spectrum was recorded approximately 30 minutes after addition of *N*-Benzylidene benzylamine and shows some conversion to a new paramagnetic product. The NMR tube was left at room temperature after which the solution color changed from dark purple to dark red and a precipitate formed. The solution was emptied into a 4 mL scintillation vial and subsequently pipetted into a clean J. Young NMR tube and a ^{1}H NMR spectrum was recorded showing an intractable mixture of paramagnetic products, none of which could be identified. To the NMR tube with the remaining

solids was added approximately 0.5 mL thf and a thf-d_8 capillary resulting in a light red solution. A ^{1}H NMR spectrum of this solution was recorded but no resonances other than solvent resonances were visible.

3.9 Reaction of 2 with $B(C_6F_5)_3$. In a 20 mL scintillation vial, 11.7 mg **2** (0.1 mmol) was dissolved in approximately 0.5 mL benzene. In a separate 4 mL scintillation vial 5.1 mg $B(C_6F_5)_3$ (0.1 mmol) was dissolved in minimal benzene and added to the benzene solution of **2** and the vial was swirled a few times to ensure proper mixing of reagents. An immediate color change to red was observed concomitant with deposition of a black oil. The solution was left at room temperature for one day after which the black oil hardened somewhat. The solvent was removed *in vacuo* and the combined solids dissolved in approximately 0.5 mL thf and added to a J. Young NMR tube equipped with a thf-d_8 capillary. A ^{1}H NMR spectrum was recorded which showed the formation of a new paramagnetic molecule(s) as evidenced by many sharp resonances. An ^{11}B NMR resonance was recorded which showed three resonances. While a reaction occurred, it clearly did not result in the formation of **3**.

3.10 Reaction of 2 with acetonitrile. In a 20 mL scintillation vial, 11.7 mg **2** (0.1 mmol) was dissolved in approximately 0.5 mL benzene to this solution was added a few drops of acetonitrile resulting in an immediate color change to red. The solution was left at room temperature for one day after which no visible changes were observed. The solvents were removed *in vacuo* and the remaining solid dissolved in thf and added to a J. Young NMR tube equipped with a thf-d_8 capillary. A ^{1}H NMR spectrum was recorded which showed the formation of a new paramagnetic molecule. While a reaction occurred, it clearly did not result in the formation of **3**.

3.11 Reaction of 3 with chlorocatechol borane to form 5 and phenylcatechol borane (6). In a 4 mL scintillation vial, 8.8 mg **3** (0.1 mmol) was dissolved in approximately 0.5 ml thf and this solution was transferred to a J. Young NMR tube. A thf-d_8 capillary was added to the NMR tube and an initial ^{1}H NMR spectrum was recorded. Concurrently, a ^{11}B NMR spectrum of chlorocatechol borane (ClBCat) was recorded in thf with a thf-d_8 capillary. The NMR tube containing **3** was returned to the glovebox. In a 4 mL scintillation vial, 1.5 mg ClBCat (0.1

mmol) was dissolved in minimal thf and this solution was added to the NMR tube containing **3**. No obvious color change was noticed following ClBCat addition. The NMR tube was carefully inverted a few times to ensure proper mixing of reagents. Approximately one hour later, another ^{1}H NMR spectrum was recorded showing clean conversion to **5**. ^{11}B NMR spectroscopy recorded approximately one hour after ClBCat addition shows one broad resonance at 32.6 ppm consistent with the formation of **6**.[11]

3.12 Reduction of 5 to regenerate 2. In a 20 mL scintillation vial, 10.4 mg **5** (0.01 mmol) was dissolved in approximately 6 mL toluene equipped with a magnetic stir bar. In a 4 mL scintillation vial, 2.6 mg 18-crown-6 (0.01 mmol) was dissolved in 2 mL toluene. This 18-crown-6 toluene solution was pipetted into another 4 mL scintillation vial containing an excess of 6.9 mg KC_8 (0.51 mmol). This combined KC_8/18-crown-6 solution was added to the toluene solution of **5** while stirring at room temperature. The vial containing the combination of KC_8/18-crown-6 was rinsed with one pipette toluene and the washings were added to the reaction mixture. The reaction mixture was stirred at room temperature for one hour during which a gradual color change from orange to dark purple was observed. The reaction mixture was filtered through a plug of celite and eluted with an additional 2 mL toluene. The filtered solution was concentrated to approximately 0.5 mL and placed in a -35 °C freezer to crystallize overnight. Large, dark purple/black crystals formed overnight and were collected by decanting the supernatant followed by drying the crystals under vacuum. While the mass of crystals was too small to measure, we were able to obtain a ^{1}H NMR spectrum of this material showing the clean formation of **2**.

3.13 Statement on purity of compounds. There has been much debate on the usefulness of elemental analysis as a metric of compound purity and composition.[12–14] Recent studies have found this technique prone to random error[15] and data manipulation.[16] Due to the air sensitivity and instability of compounds **2**, **3**, **4**, and **5**, we were unable to obtain satisfactory elemental analysis for these compounds. Instead, we had to establish bulk purity and structural confirmation by other means. The structures of **2**, **3**, **4**, and **5** could be unambiguously determined by X-Ray crystallography and the symmetry, bulk purity, and number of proton

environments of **2**, **3**, and **5** confirmed by ^{1}H NMR spectroscopy. The isolation of pure **4** eluded us unfortunately, likely due to the instability of boron hydride compounds. The bulk purity of **2**, **3** and **5** can be observed in reproducible and clean DC SQUID and ^{57}Fe Mössbauer data which give results consistent with each other (and with a solution state magnetic moment determined by the Evans Method). The N – N stretch in **2** can be easily located in the IR spectrum at 1851 cm^{-1}.

4 ^{1}H NMR Spectroscopy

4.1 ^{1}H NMR spectrum of 2

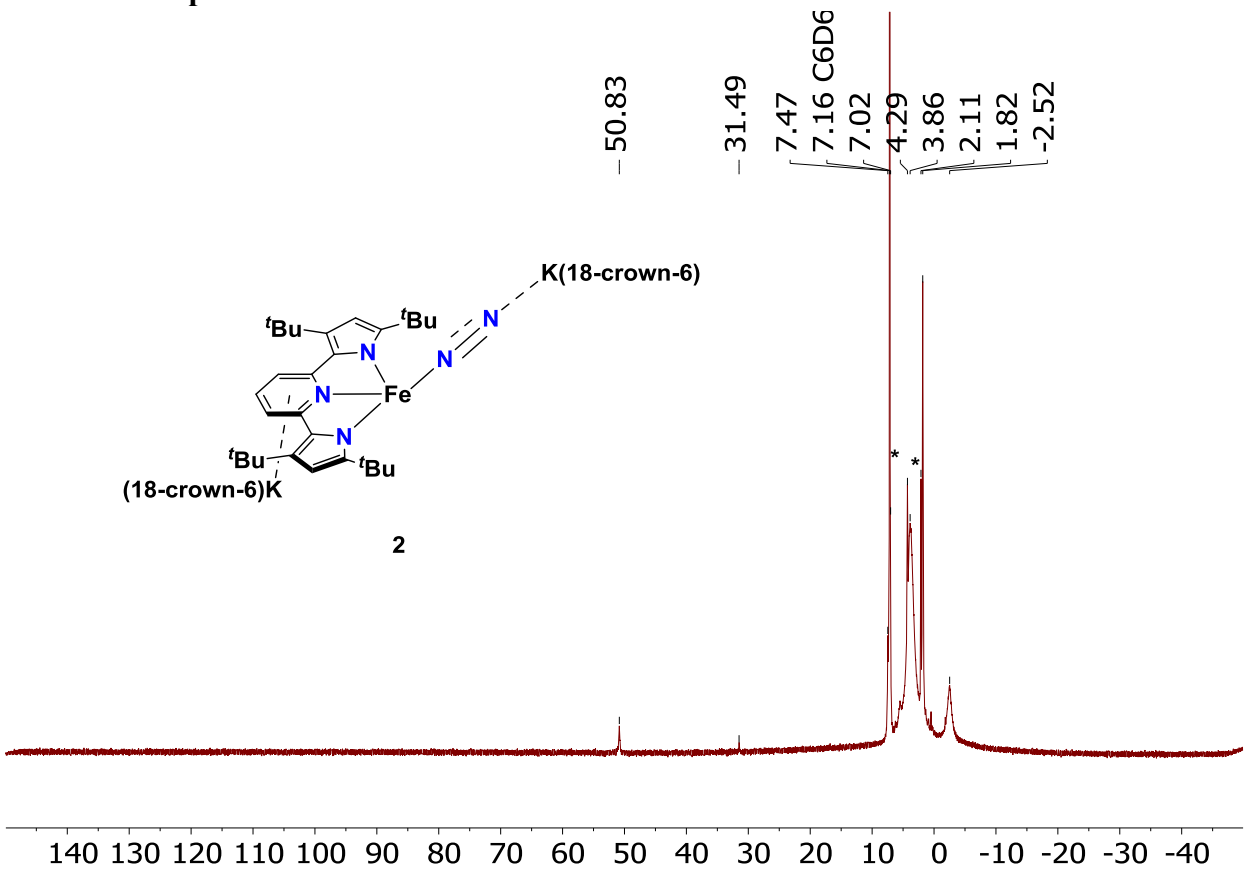

Figure S1. ^{1}H NMR spectrum of [{K(18-crown-6)}$_2$(^{tBu}pyrr$_2$pyr)Fe(N$_2$)] (**2**). Residual toluene from crystallization is labelled as "*". (500 MHz, C_6D_6, 298 K)

4.2 ^{1}H NMR spectrum of 3

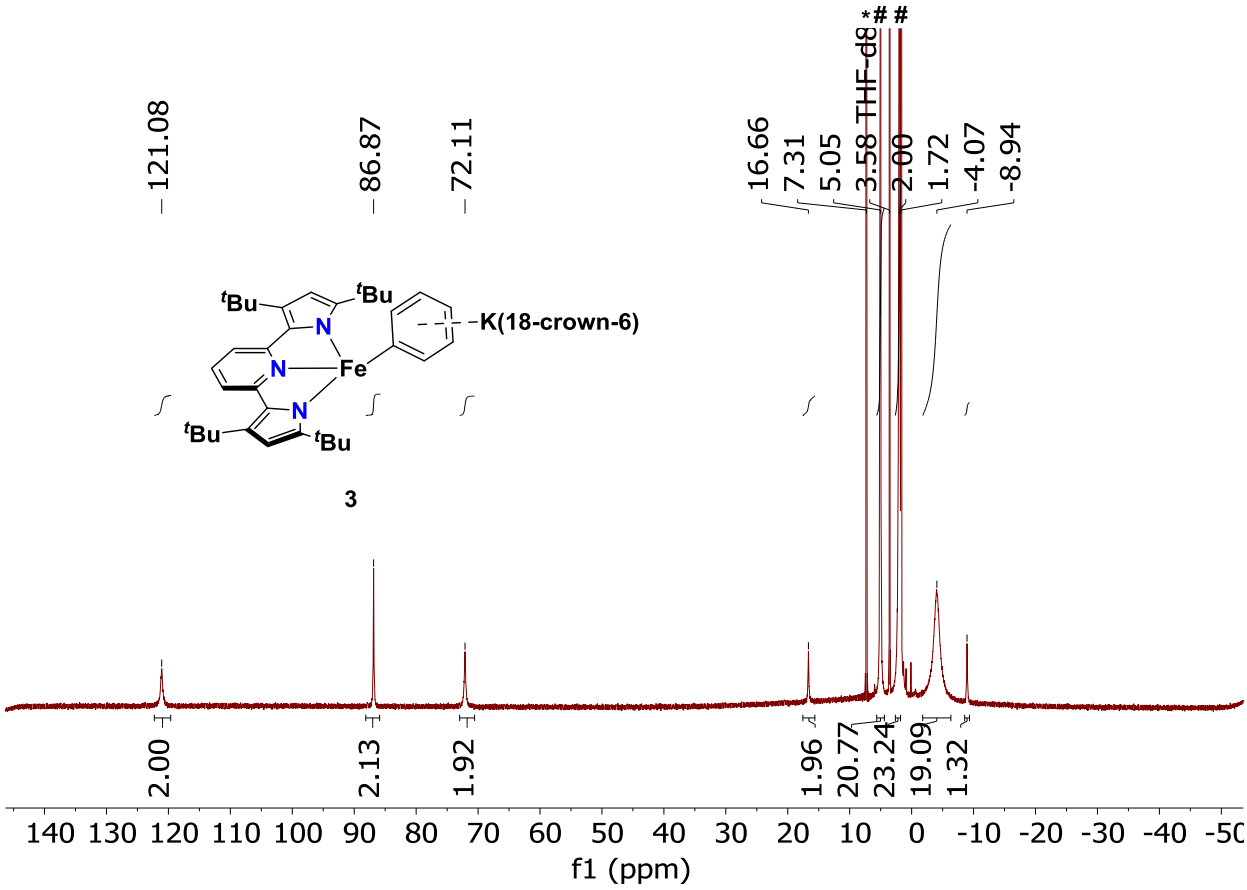

Figure S2. ^{1}H NMR spectrum of [{K(18-C-6)}($^{t\text{Bu}}$pyrr$_2$pyr)Fe(C_6H_5)] (**3**). Cocrystallized benzene is labelled as "*" and the residual thf-H_8 peaks are labelled as "#". (500 MHz, thf-d_8, 298 K)

4.3 ^{1}H NMR spectrum of 5 in thf-d_8

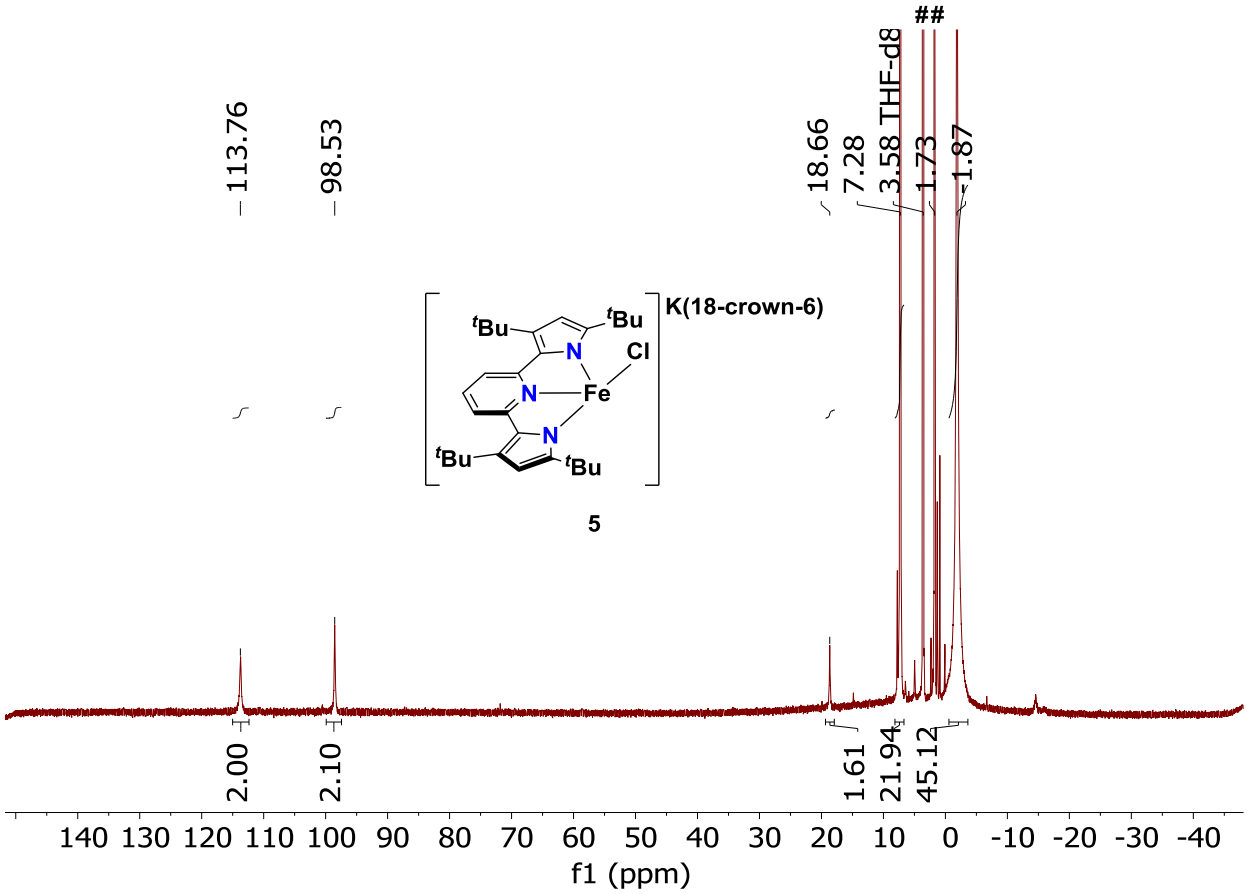

Figure S3. ^{1}H NMR spectrum of [{K(18-crown-6)(thf)$_2$}($^{t\text{Bu}}$pyrr$_2$pyr)FeCl] (**5**). Residual thf-H_8 peaks are labelled as "#". (500 MHz, thf-d_8, 298 K)

4.4 ^{1}H NMR spectrum of 5 in C_6D_6

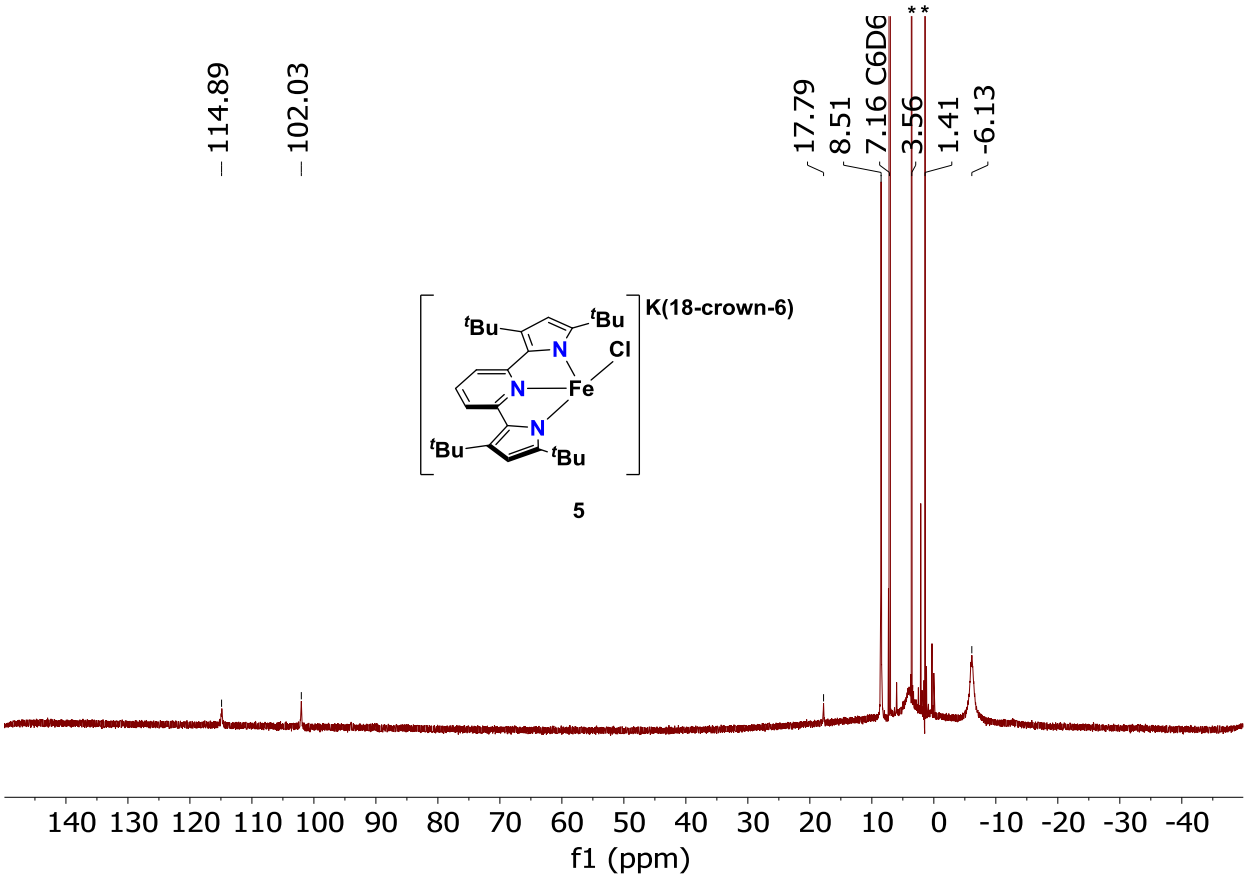

Figure S4. ^{1}H NMR spectrum of [{K(18-crown-6)(thf)$_2$}($^{t\text{Bu}}$pyrr$_2$pyr)FeCl] (**5**). Residual thf-H_8 peaks are labelled as "*". (500 MHz, C_6D_6, 298 K)

5 Reactions Monitored by ^{1}H NMR Spectroscopy

5.1 ^{1}H NMR spectrum of reaction of [{K$_2$(18-C-6)($^{t\text{Bu}}$pyrr$_2$pyr)Fe}$_2$(μ-N$_2$)] with two eq. 18-crown-6

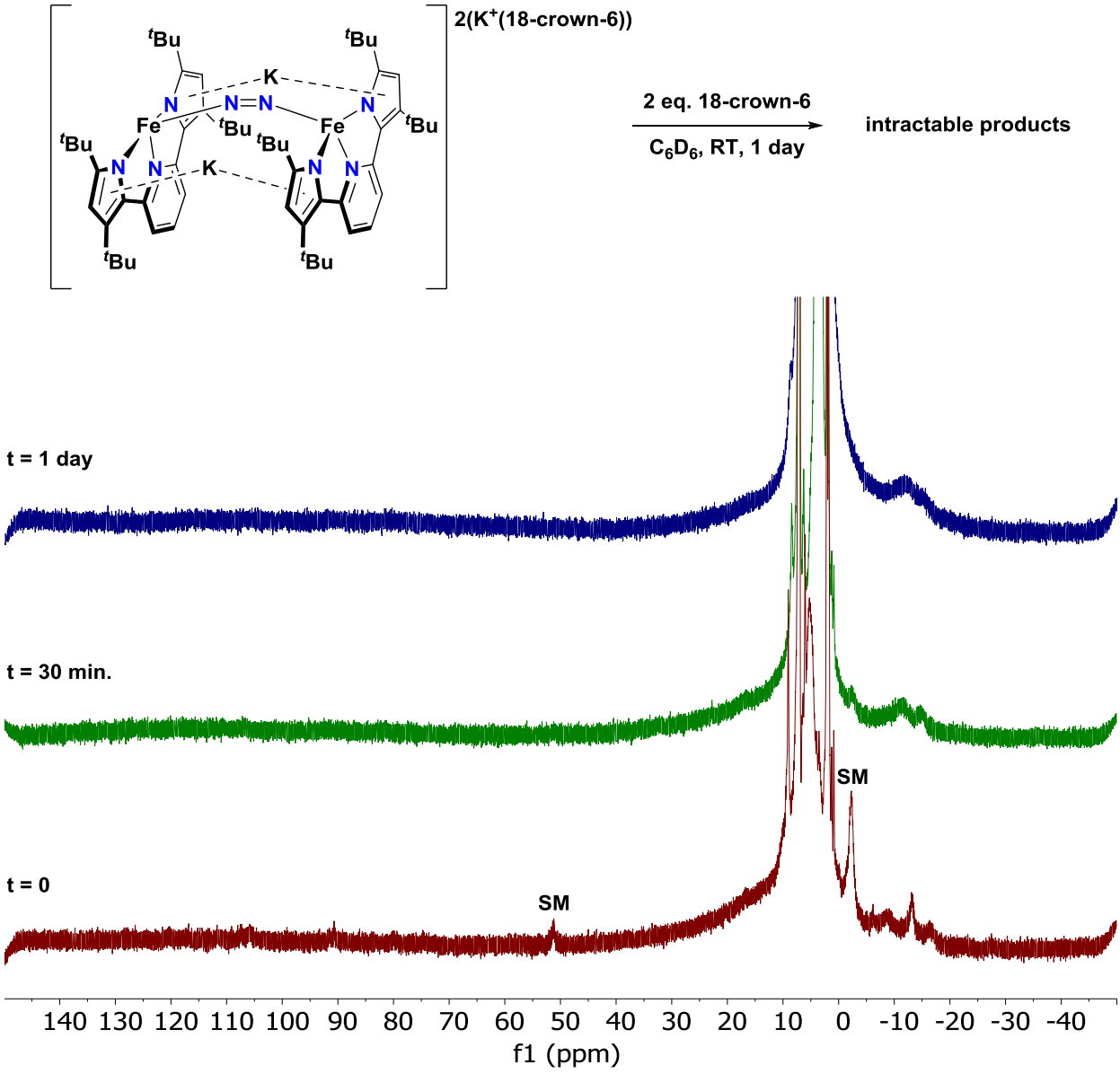

Figure S5. Stacked ^{1}H NMR spectrum of the reaction between [{K$_2$(18-C-6)($^{t\text{Bu}}$pyrr$_2$pyr)Fe}$_2$(μ-N$_2$)] (**SM**) and two equivalents of 18-crown-6. (500 MHz, C$_6$D$_6$, 298 K)

5.2 ^{1}H NMR spectrum of reaction of 1 with two eq. Me_3SiCl and 18-crown-6

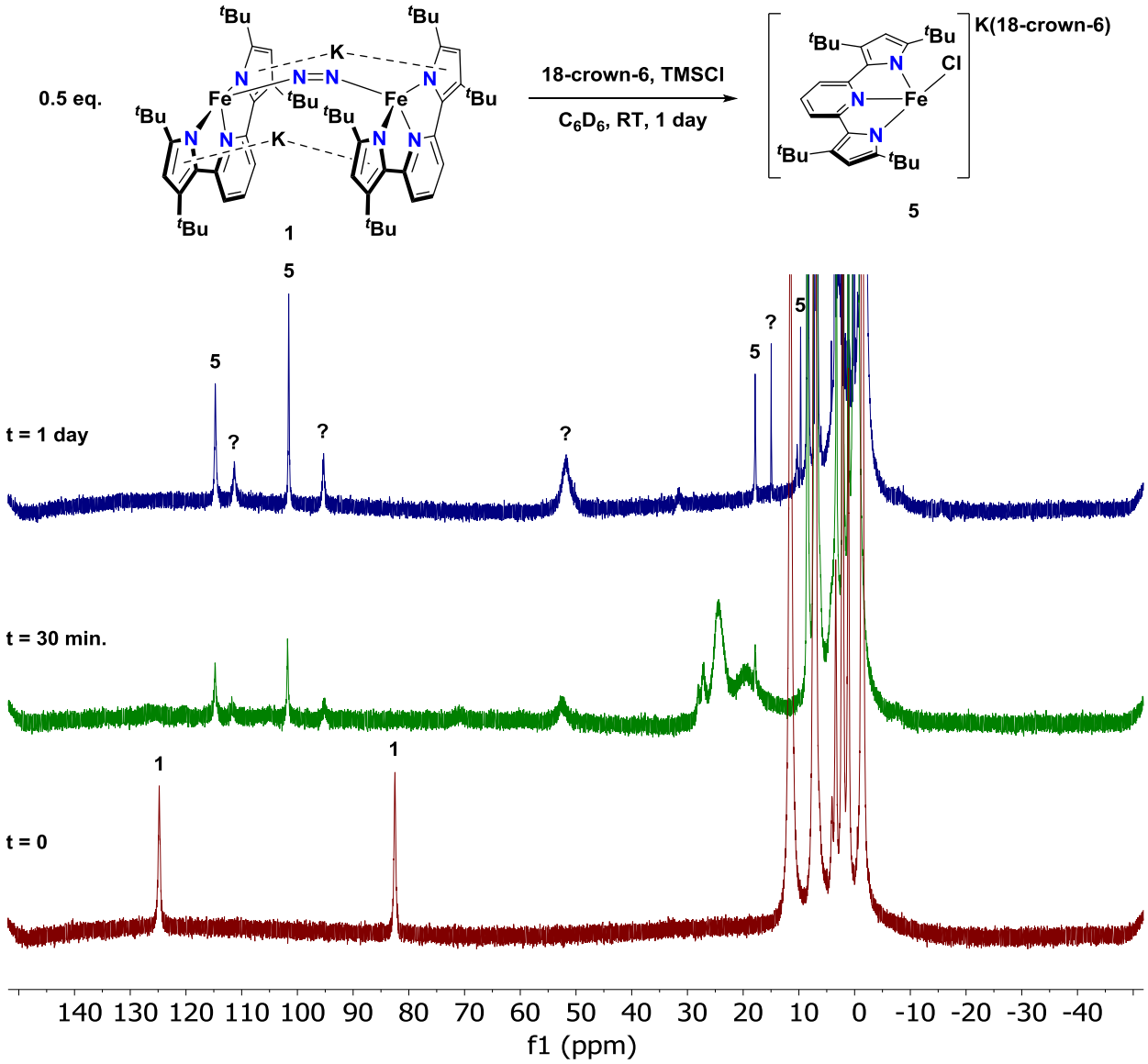

Figure S6. Stacked ^{1}H NMR spectrum of the reaction between **1** and Me_3SiCl and 18-crown-6. An unidentified side product is labelled as "**?**". (500 MHz, C_6D_6, 298 K)

5.3 ^{29}Si INEPT spectrum of reaction of 1 with two eq. Me_3SiCl and 18-crown-6

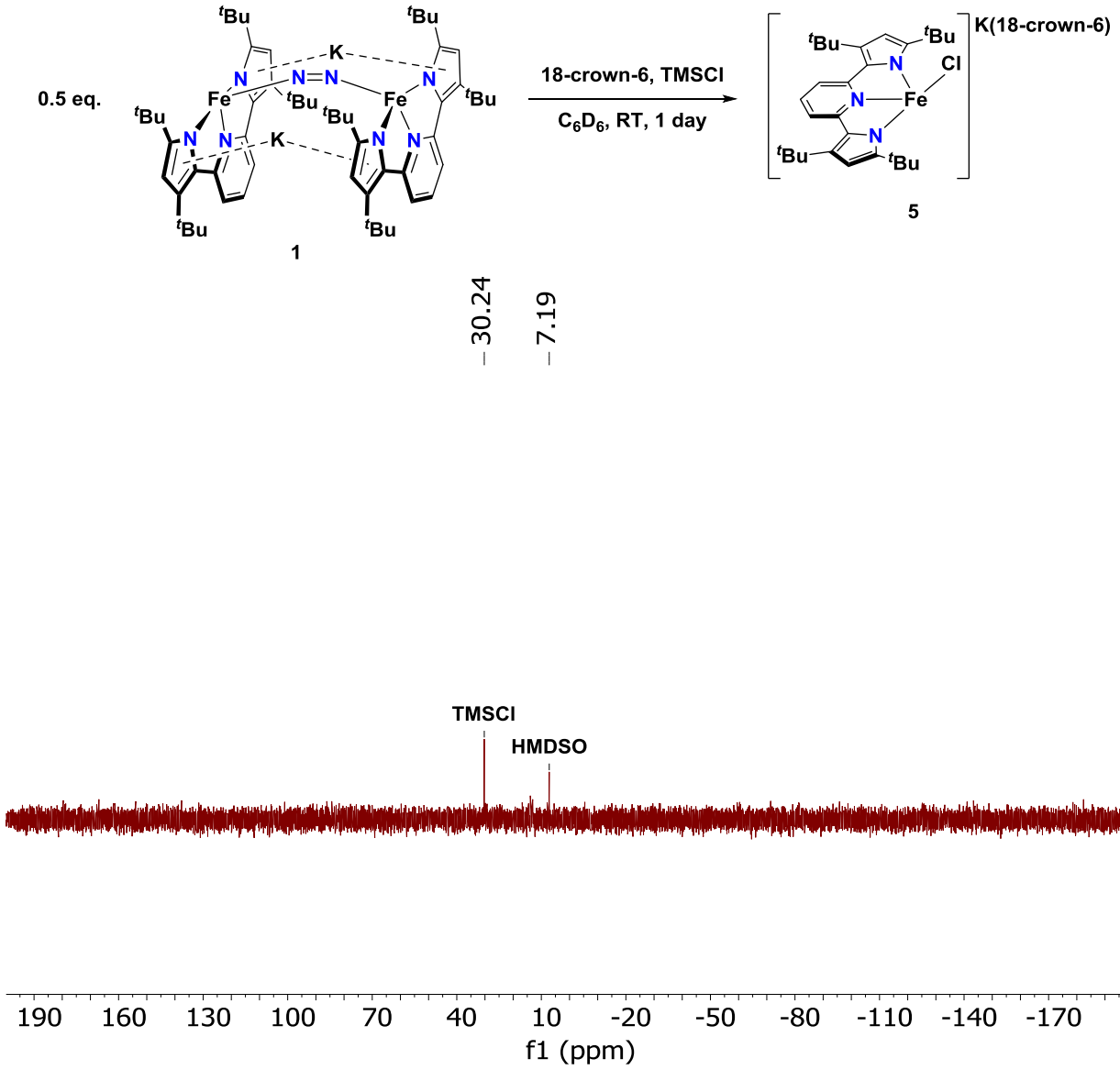

Figure S7. ^{29}Si INEPT spectrum of the reaction between **1** and Me_3SiCl and 18-crown-6 after one day. The resonance attributable to unreacted trimethyl silyl chloride is labelled as "**Me_3SiCl**" and the resonance attributable to hexamethyl disiloxane is labelled as "**HMDSO**". (500 MHz, C_6D_6, 298 K)

5.4 ^{11}B NMR spectrum of the between 2 and and B_2pin_2

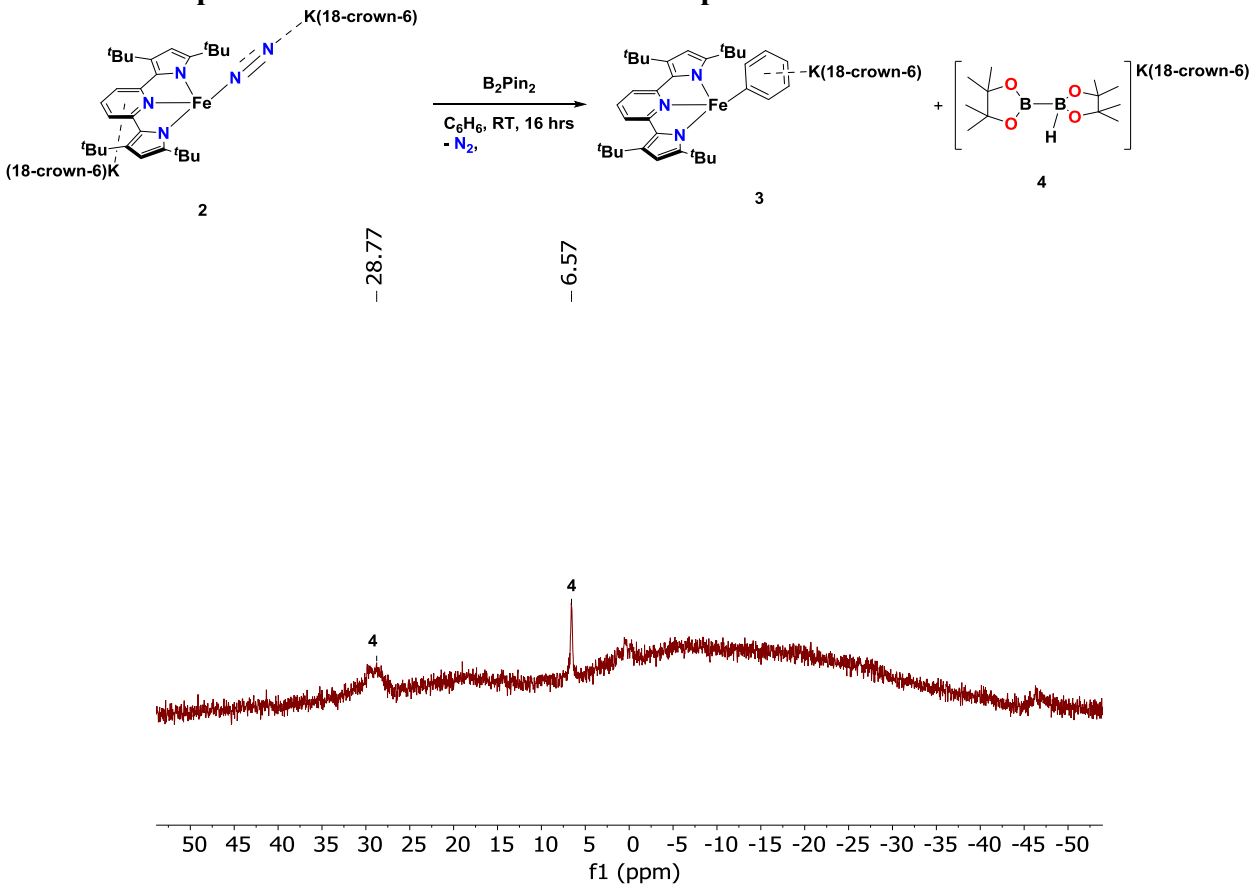

Figure S8. ^{11}B NMR spectrum of the crystalline material following the reaction between **2** and and B_2pin_2. (128 MHz, thf-d_8, 298 K)

5.5 ^{11}B NMR spectrum of the supernatant of the reaction between 2 and and B_2pin_2

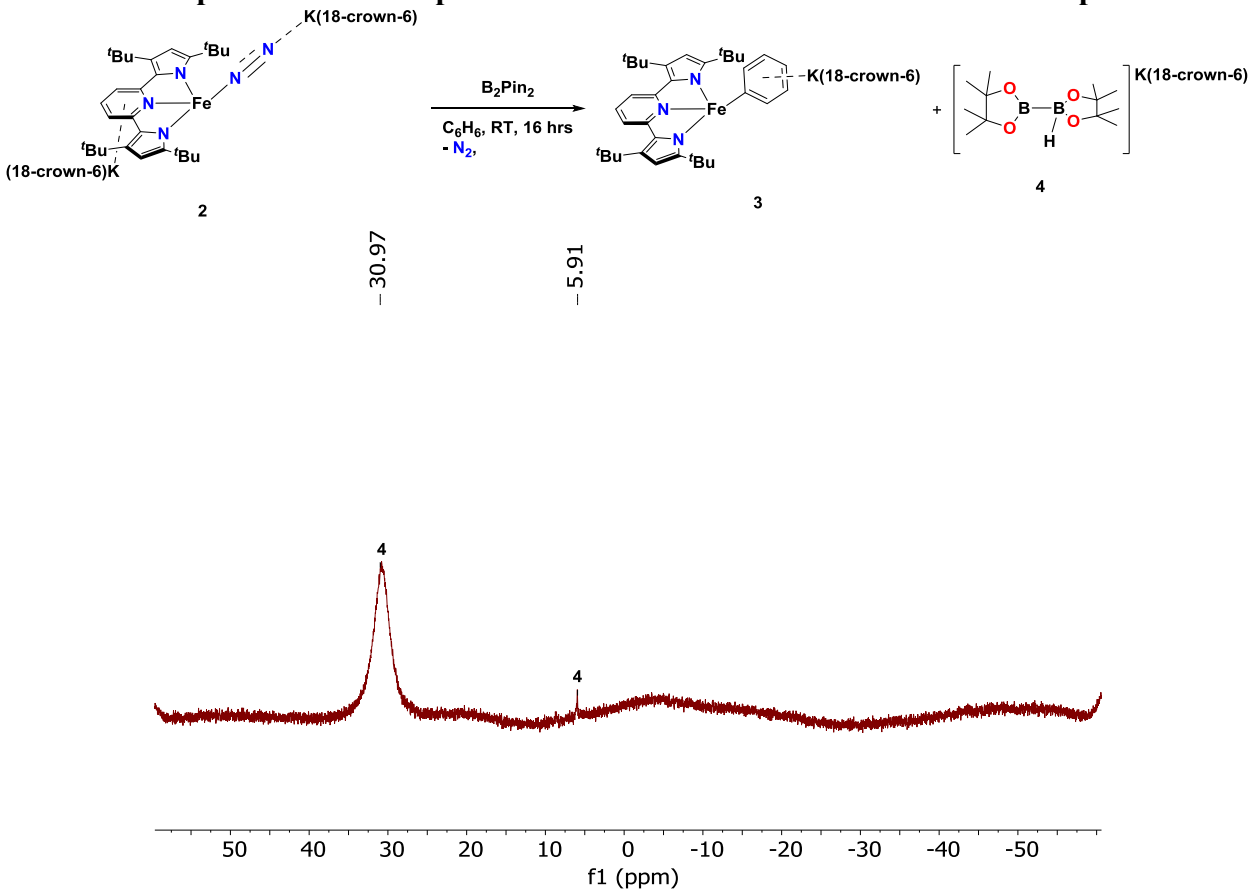

Figure S9. ^{11}B NMR spectrum of the crude supernatant following the reaction between **2** and and B_2pin_2. (128 MHz, thf-d_8, 298 K)

5.6 ^{1}H NMR spectrum of reaction of 2 with fluorobenzene

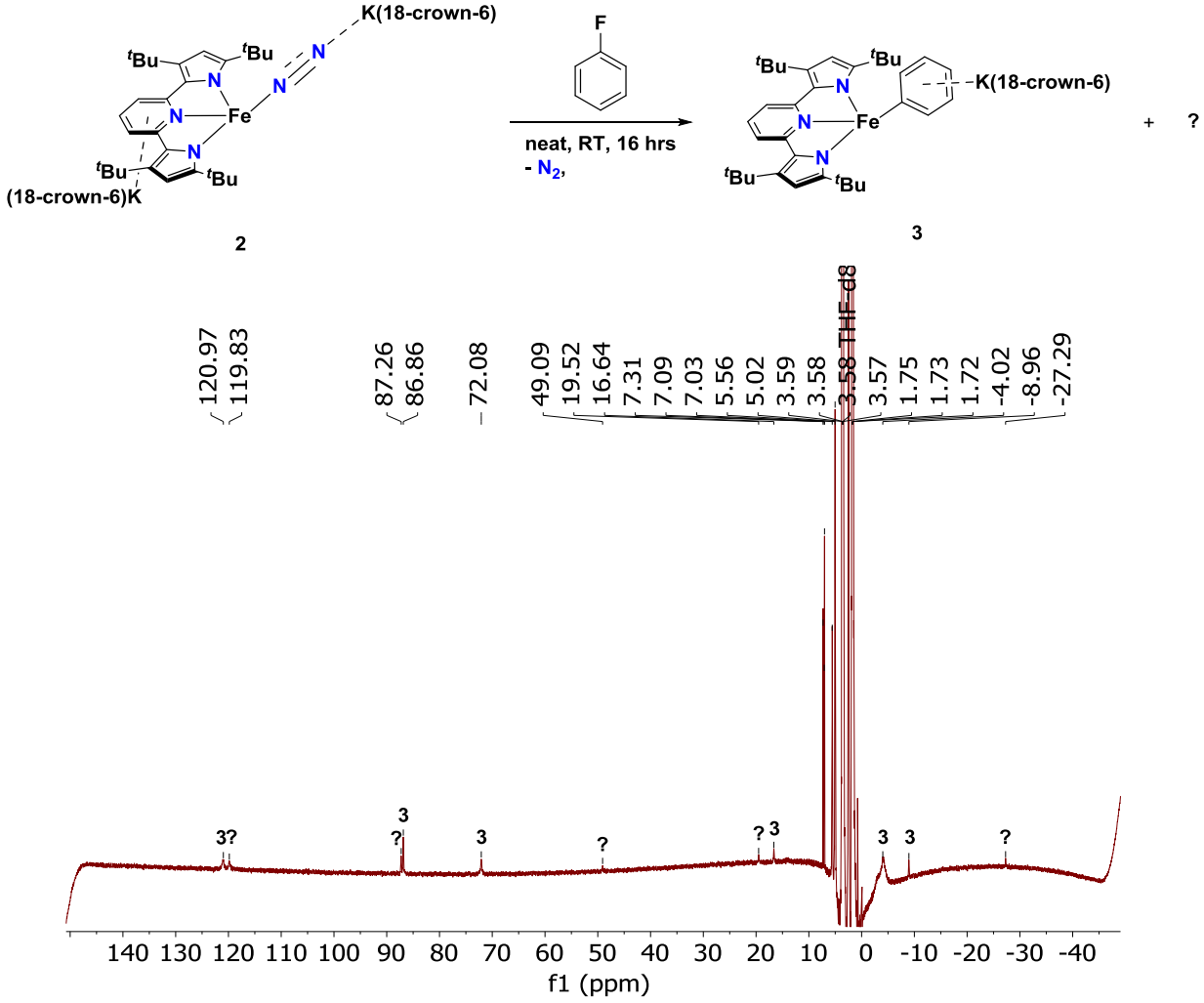

Figure S10. ^{1}H NMR spectrum of crystalline material obtained from reaction of **2** with fluorobenzene. Resonances attributable to **3** are labelled as such and resonances of an unidentified paramagnetic molecule are labelled as "**?**". (500 MHz, thf-d_8, 298 K)

5.7 ^{1}H NMR spectrum of supernatant from reaction of 2 with fluorobenzene

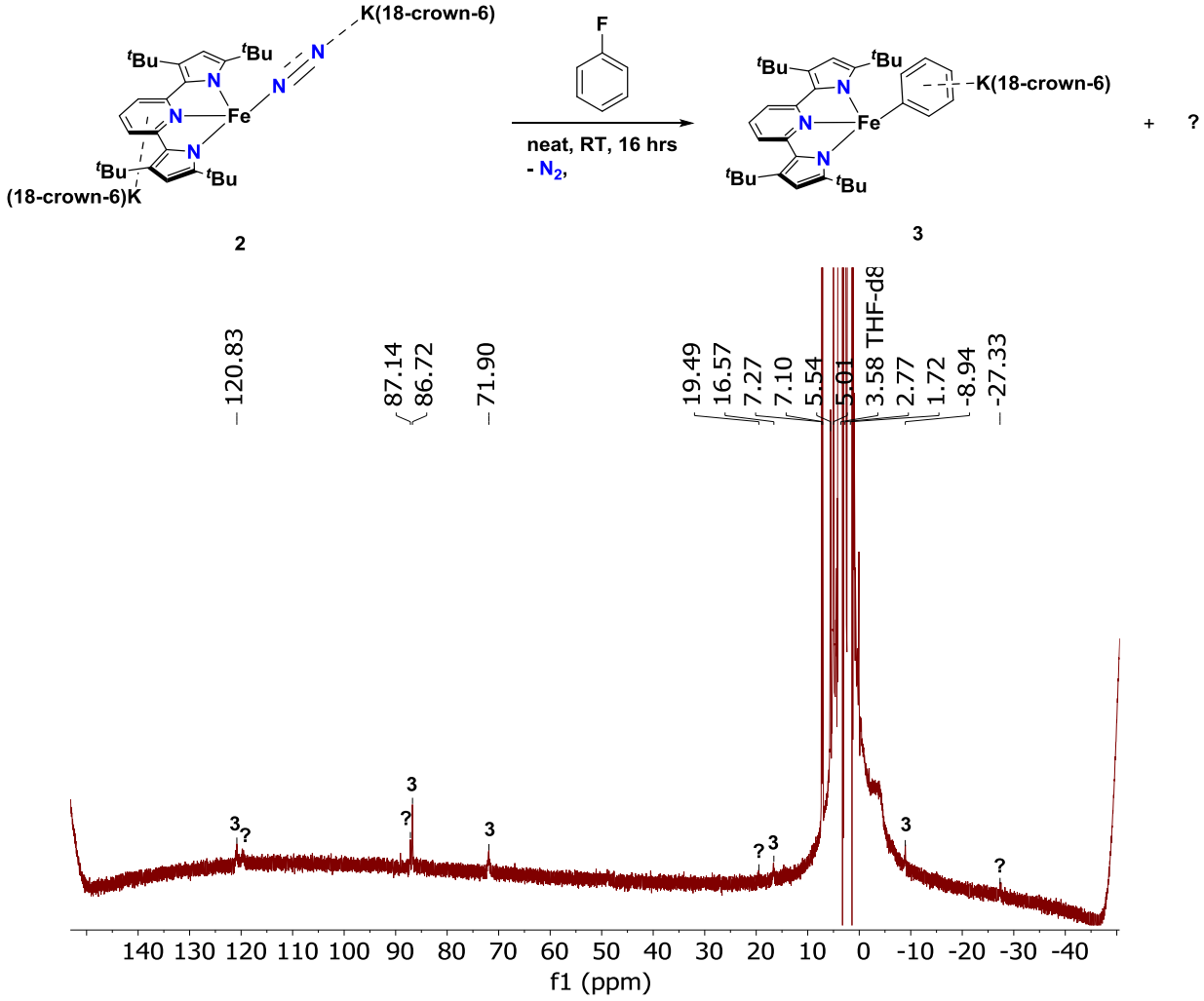

Figure S11. ^{1}H NMR spectrum of supernatant obtained from reaction of **2** with fluorobenzene. Resonances attributable to **3** are labelled as such and resonances of an unidentified paramagnetic molecule are labelled as "**?**". (500 MHz, thf-d_8, 298 K)

5.8 ^{19}F NMR spectrum of supernatant from reaction of 2 with fluorobenzene

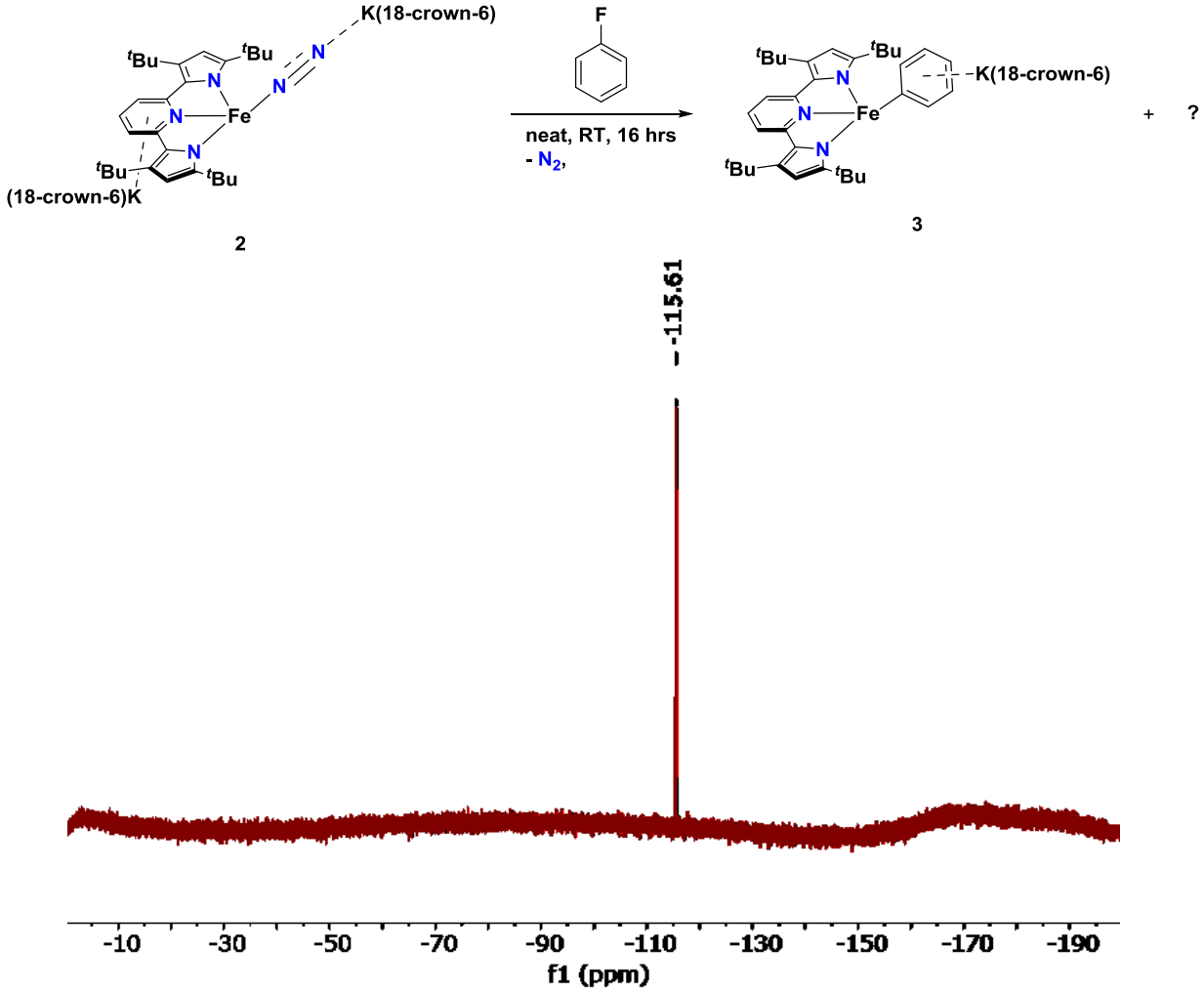

Figure S12. ^{19}F NMR spectrum of supernatant obtained from reaction of **2** with fluorobenzene. (500 MHz, thf-d_8, 298 K)

5.9 ^{1}H NMR spectrum of reaction of 2 with *N*-Benzylidene benzylamine

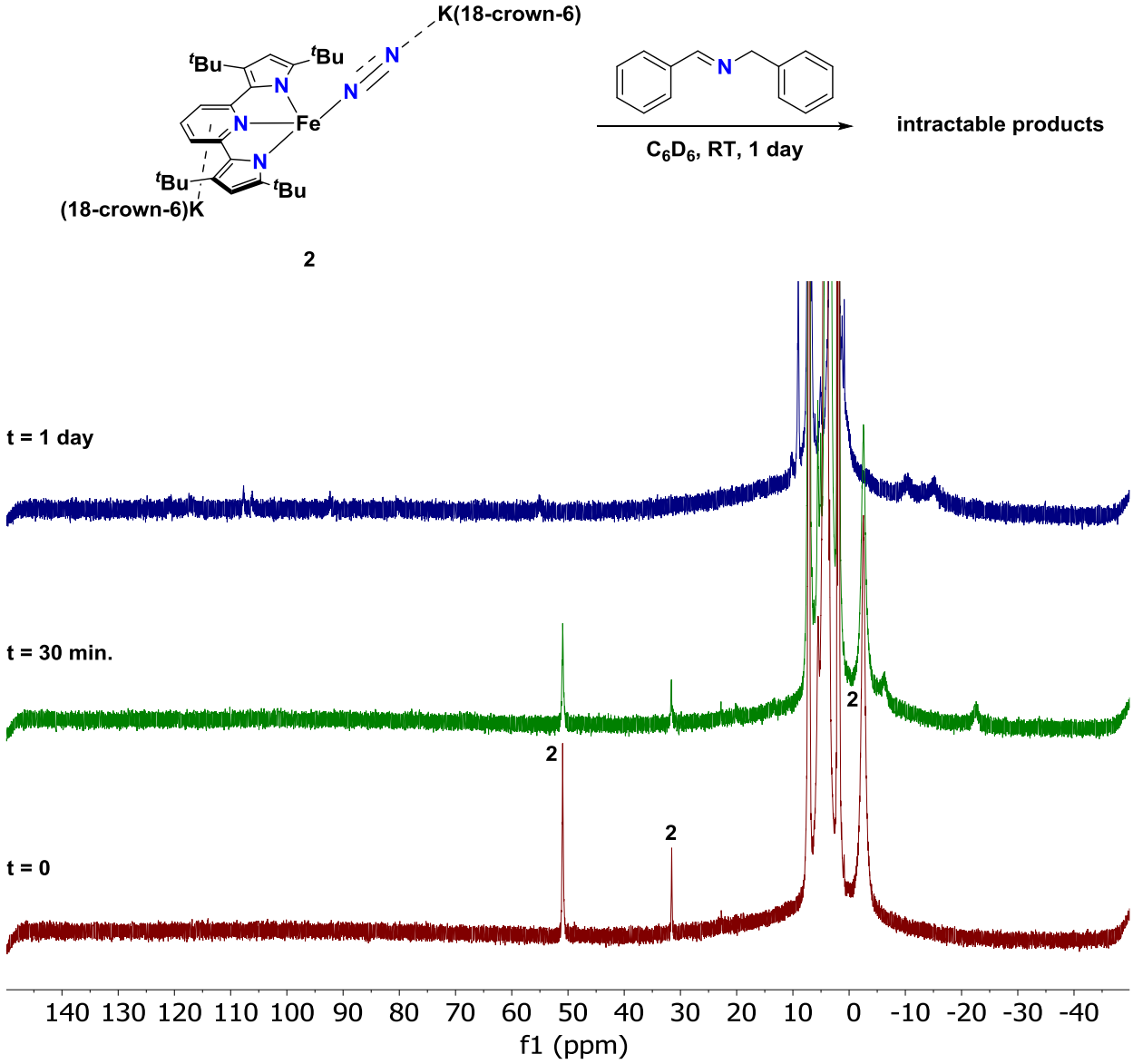

Figure S13. ^{1}H NMR spectrum from reaction of **2** with *N*-Benzylidene benzylamine. Resonances attributable to **2** are labelled. Conversion to intractable products was observed. (500 MHz, C_6D_6, 298 K)

5.10 ^{1}H NMR spectrum of solids from reaction of 2 with *N*-Benzylidene benzylamine

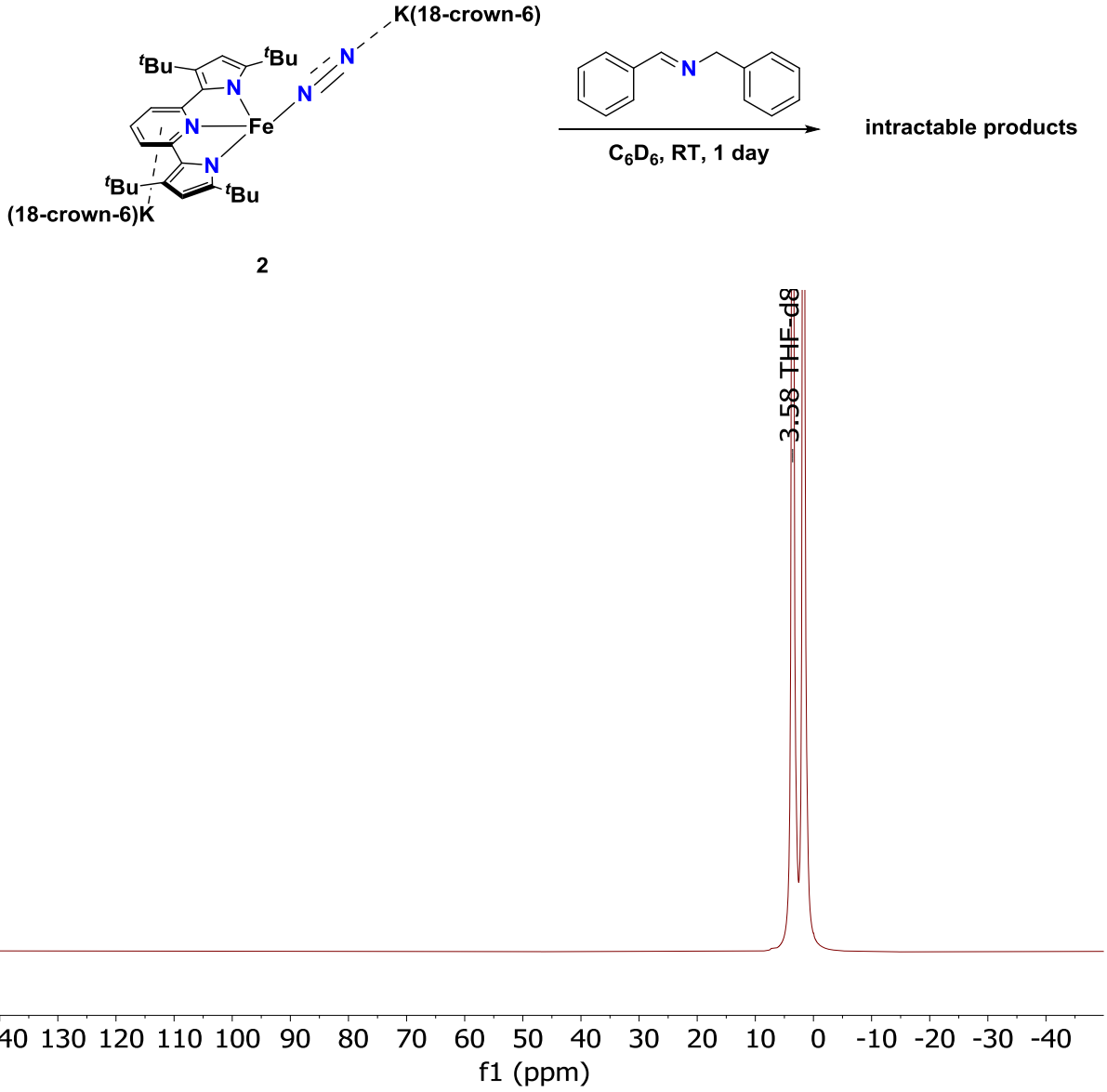

Figure S14. ^{1}H NMR spectrum from reaction of **2** with *N*-Benzylidene benzylamine of solid products dissolved in thf with a thf-d_8 capillary. No iron-containing products could be identified from this solution. (500 MHz, thf-d_8, 298 K)

5.11 ^{1}H NMR spectrum of solids from reaction of 2 with $B(C_6F_5)_3$

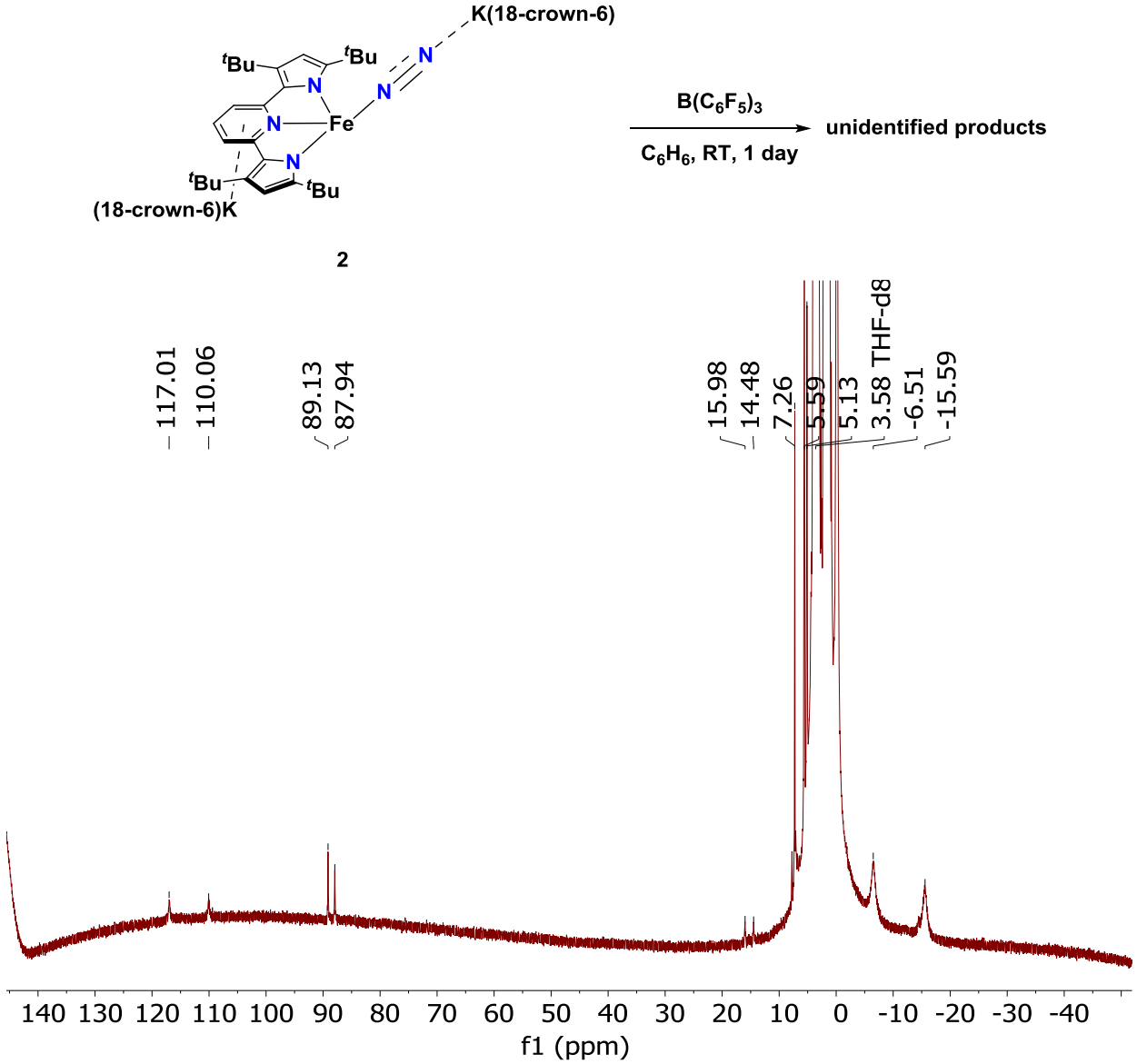

Figure S15. ^{1}H NMR spectrum from reaction of **2** with $B(C_6F_5)_3$ of solid products dissolved in thf with a thf-d_8 capillary. No iron-containing products could be identified from this solution. (500 MHz, thf-d_8, 298 K)

5.12 ^{11}B NMR spectrum of solids from reaction of 2 with $B(C_6F_5)_3$

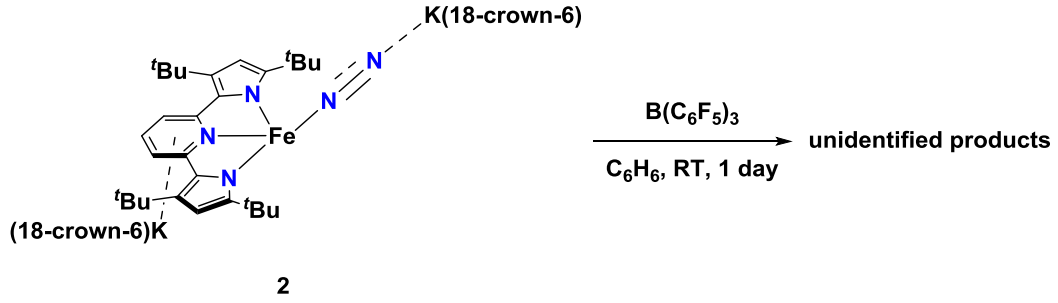

2

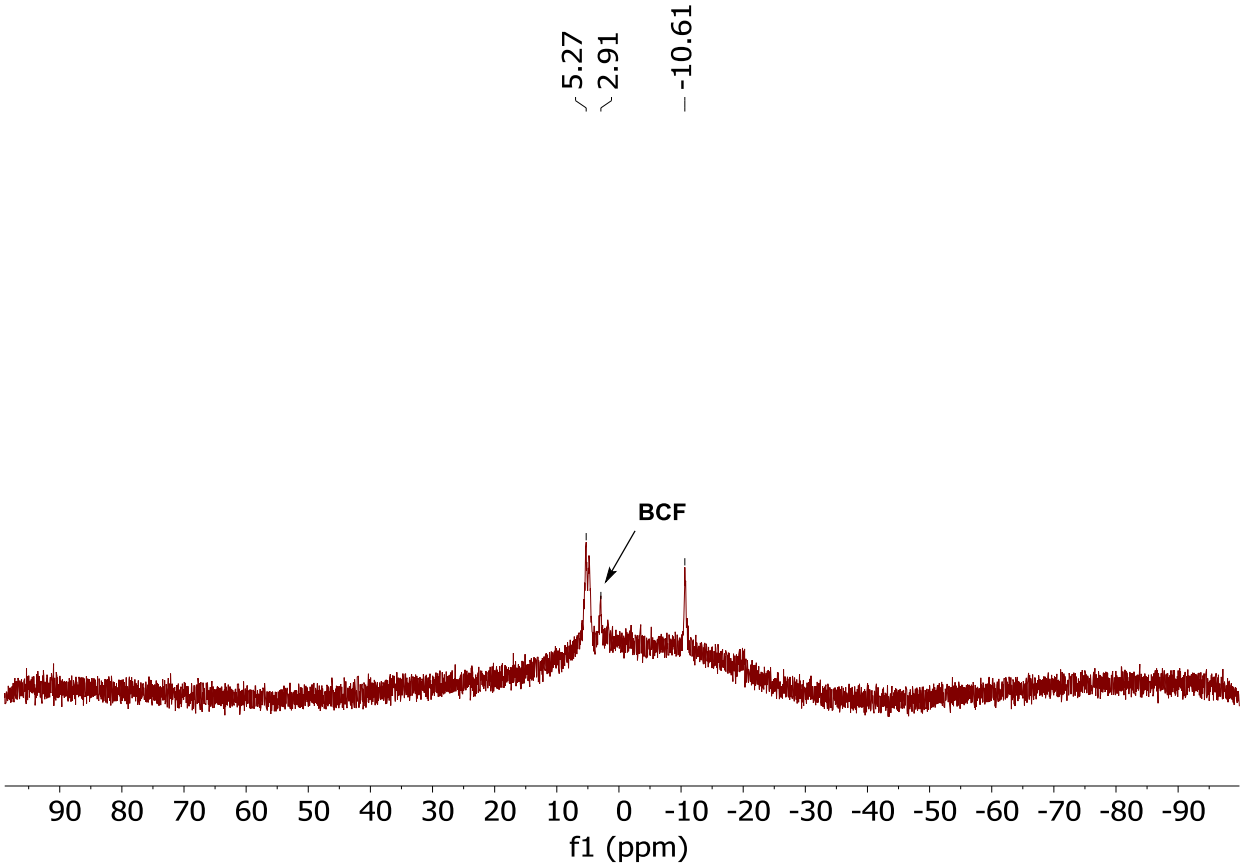

Figure S16. ^{11}B NMR spectrum from reaction of **2** with $B(C_6F_5)_3$ of solid products dissolved in thf with a thf-d_8 capillary. The resonance attributable to $B(C_6F_5)_3$ is labelled as "**BCF**". (500 MHz, thf-d_8, 298 K)

5.13 ^{1}H NMR spectrum from reaction of 2 with acetonitrile

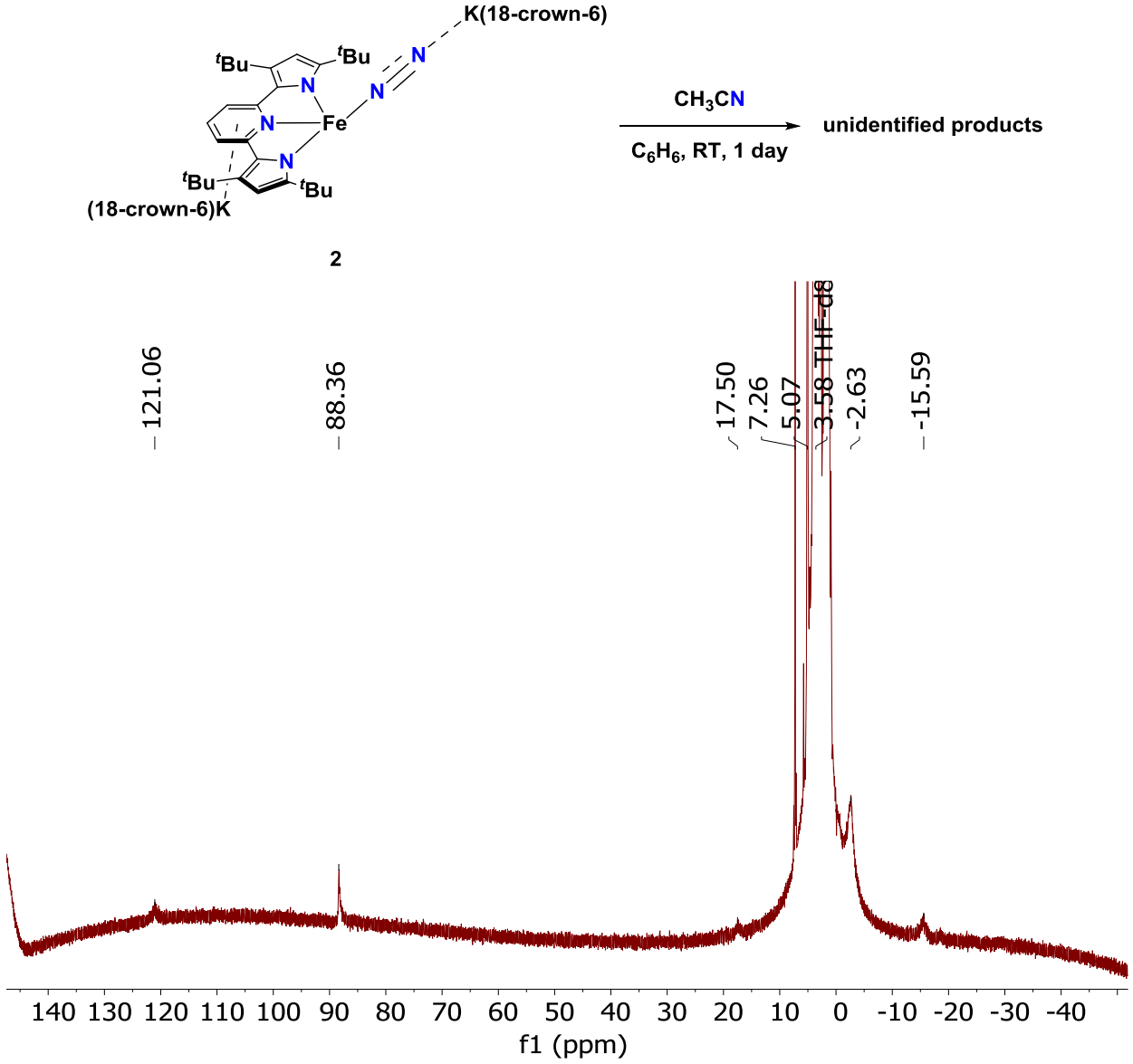

Figure S17. ^{1}H NMR spectrum from reaction of **2** with acetonitrile (CH_3CN) of solid products dissolved in thf with a thf-d_8 capillary. No iron-containing products could be identified from this solution. (500 MHz, thf-d_8, 298 K)

5.14 ^{1}H NMR spectrum of the reaction between 3 and ClBCat

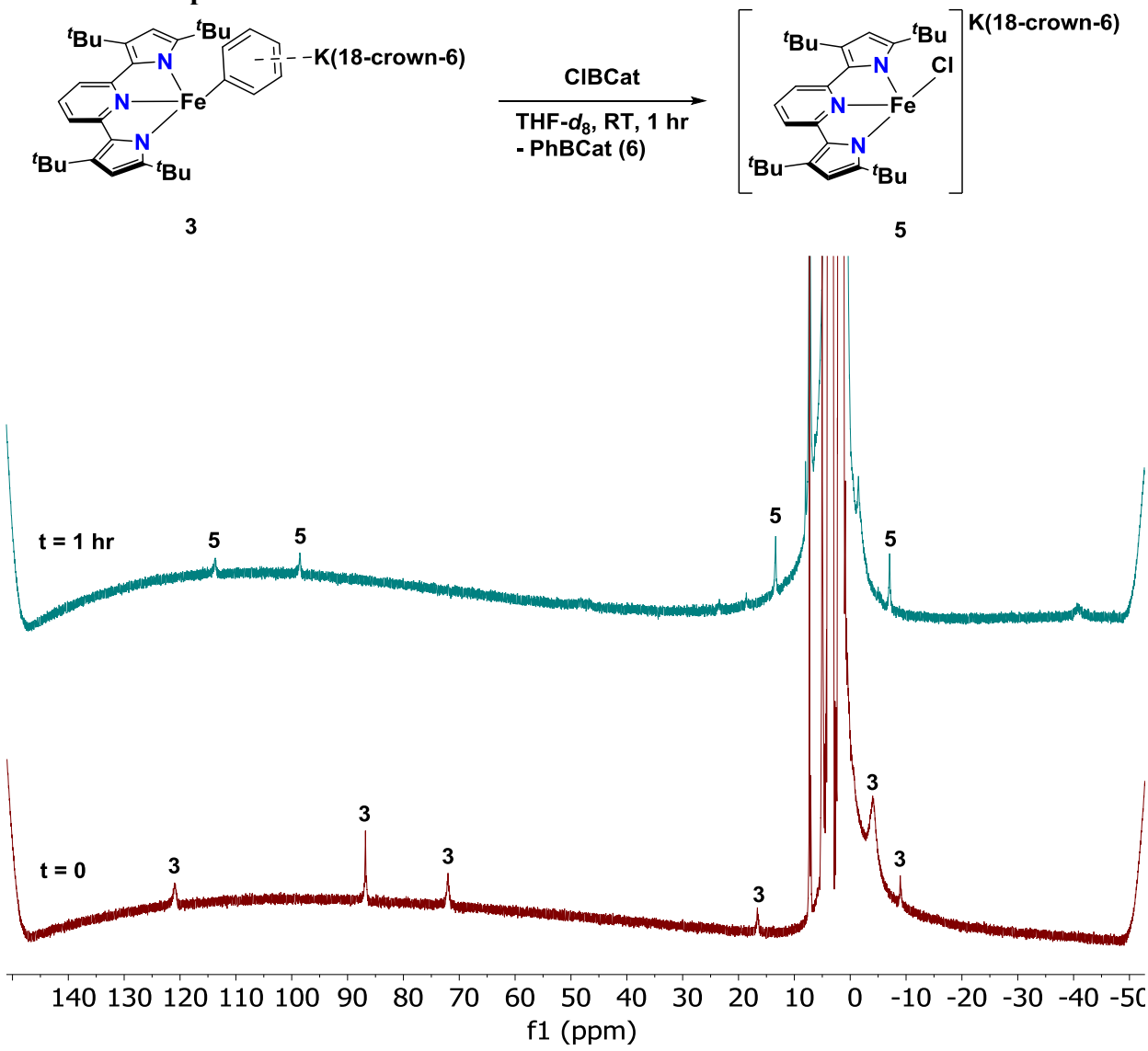

Figure S18. Stacked ^{1}H NMR spectrum of the reaction between **3** and ClBCat to form **5** and **6**. (500 MHz, thf-d_8, 298 K)

5.15 ^{11}B NMR spectrum of the reaction between 3 and ClBCat

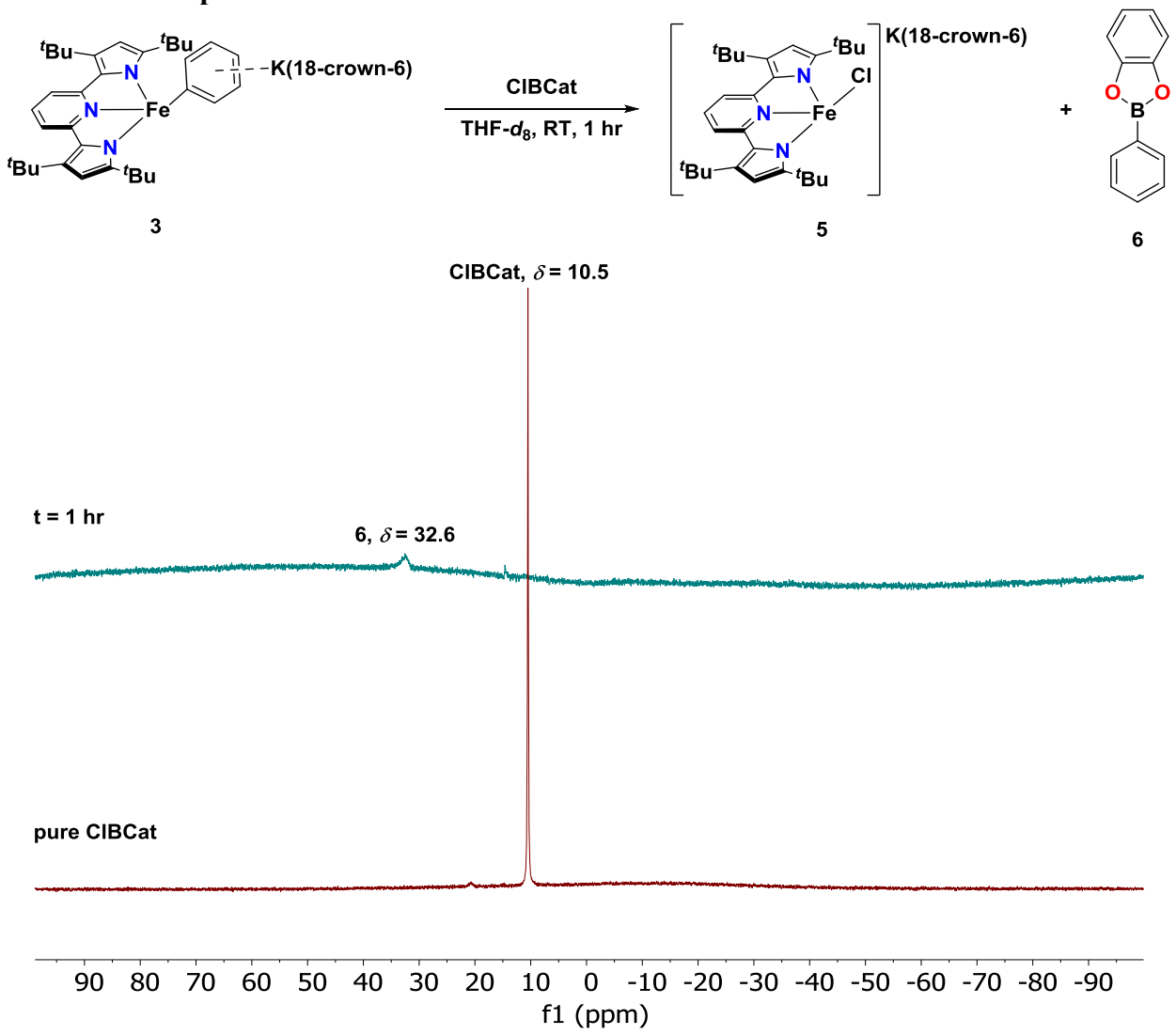

Figure S19. Stacked ^{11}B NMR spectrum of the reaction between **3** and ClBCat to form **5** and **6**. (128 MHz, thf-d_8, 298 K)

5.16 ^{1}H NMR spectrum of solids from reduction of 5 with excess KC_8 and one eq. of 18-crown-6

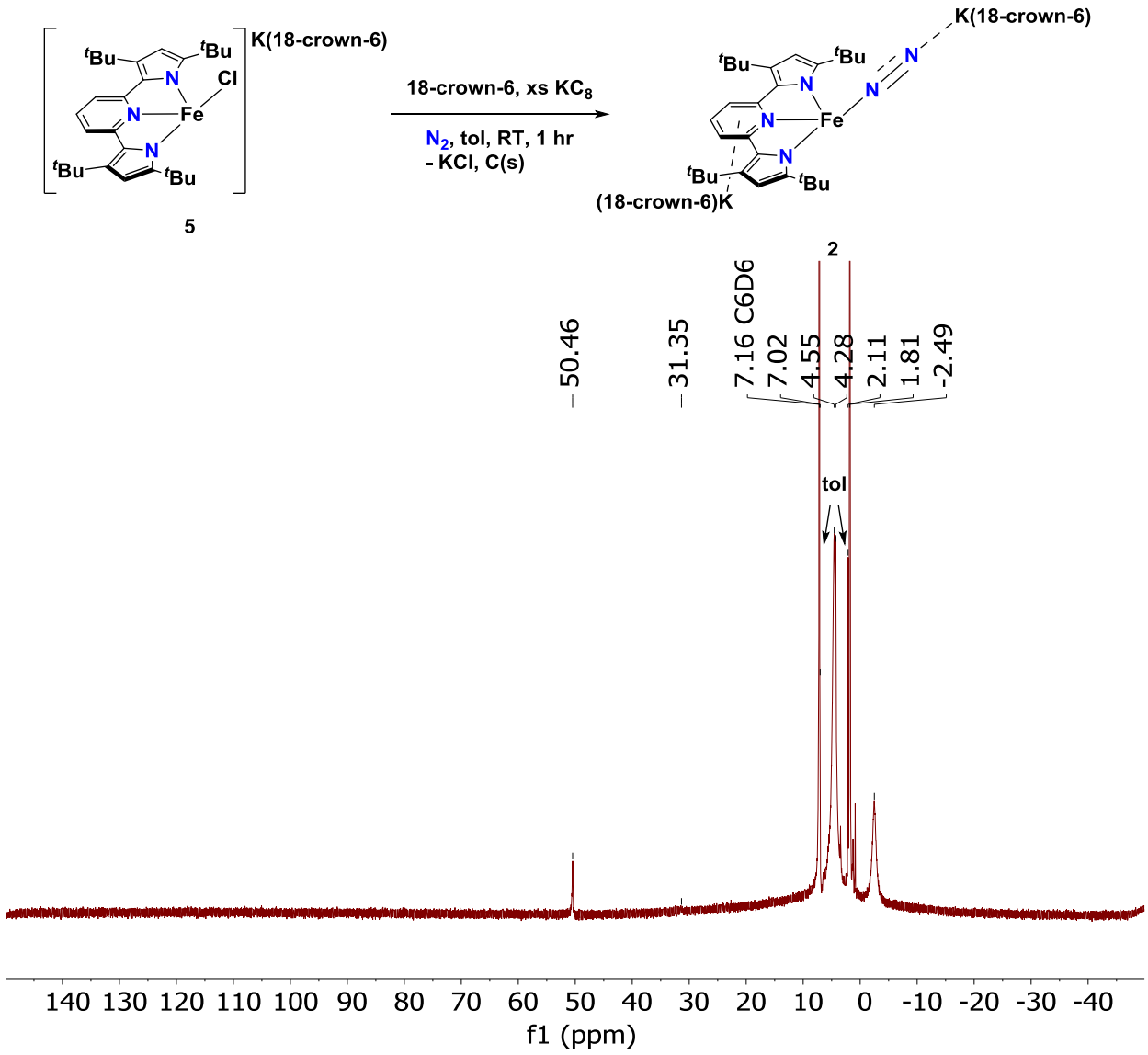

Figure S20. ^{1}H NMR spectrum of crystalline material resulting from reduction of **5** with excess KC_8 and one equivalent of 18-crown-6. The chemical shifts of this material match those of **2** perfectly with only residual toluene (**tol**) as a detectable impurity. (500 MHz, C_6D_6, 298 K)

6 IR Spectroscopy

6.1 IR Spectrum of 2

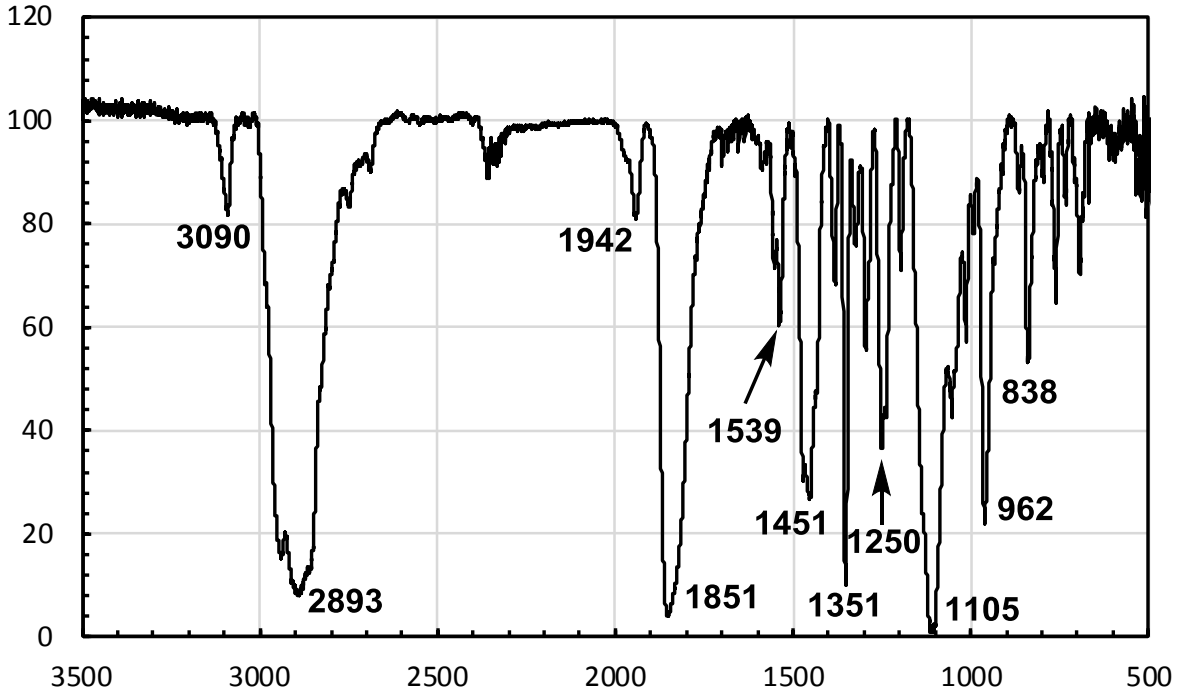

Figure S21. IR spectrum of [{K(18-crown-6)}$_2$($^{t\text{Bu}}$pyrr$_2$pyr)Fe(N$_2$)] (**2**) (solid, KBr pellet, cm^{-1}).

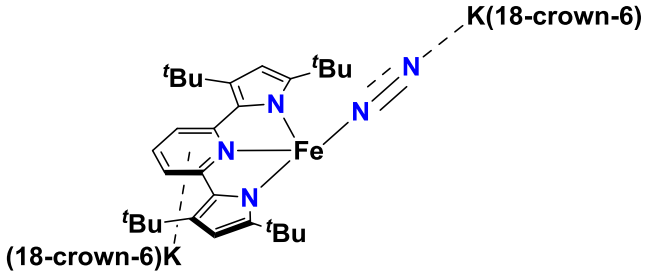

2

7 UV-Vis Spectroscopy

7.1 UV-Vis spectrum of 3

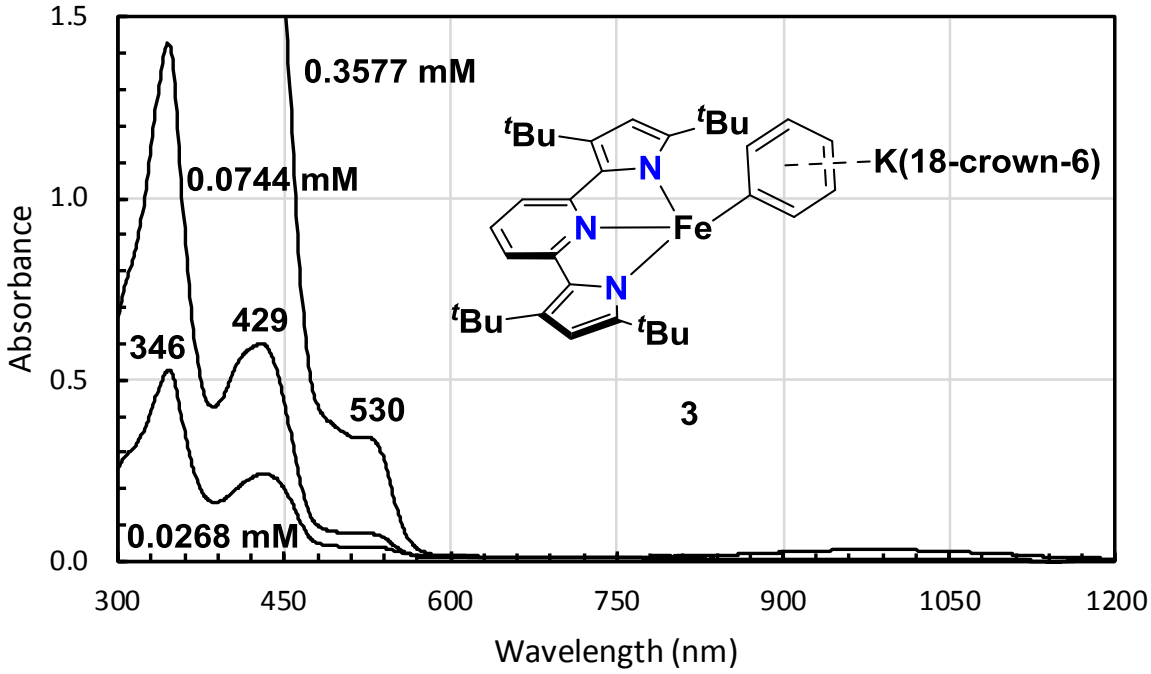

Figure S22. UV-Vis spectrum of [{K(18-C-6)}($^{t\text{Bu}}$pyrr$_2$pyr)Fe(C_6H_5)] (**3**) recorded in thf at 298 K. λ = 530 nm ε = 113 M^{-1}. λ = 429 nm ε = 8060 M^{-1}. λ = 346 nm ε = 19600 M^{-1}.

7.2 UV-Vis spectrum of 5

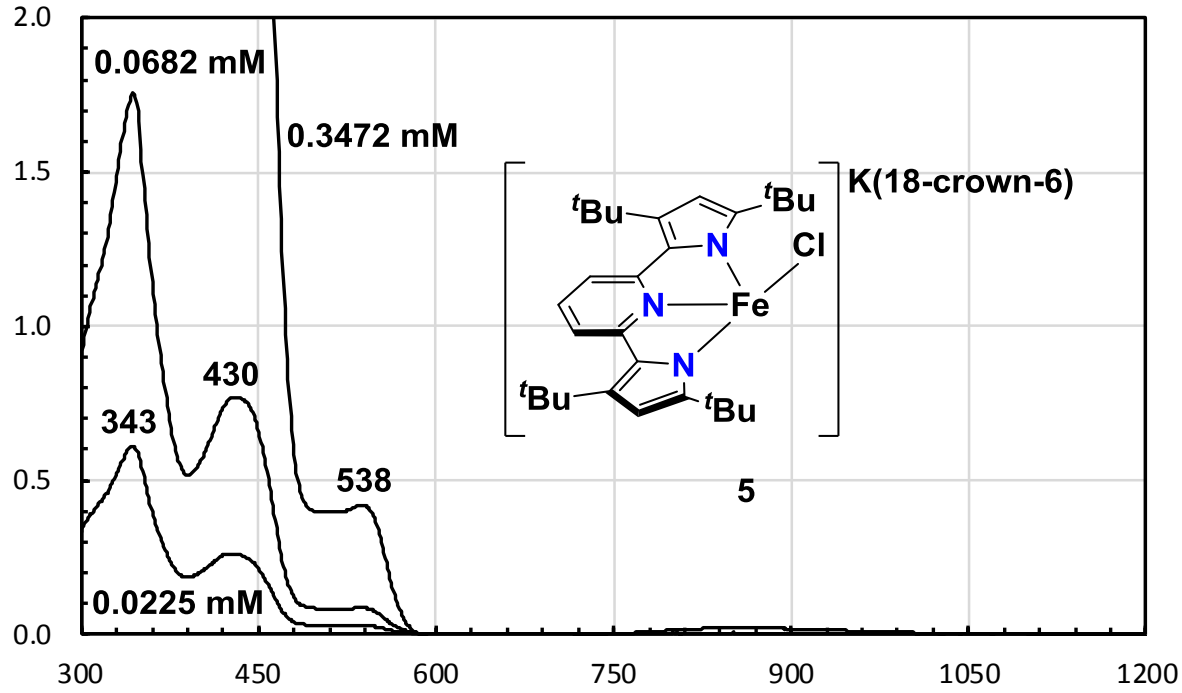

Figure S23. UV-Vis spectrum of [{K(18-crown-6)(thf)$_2$}($^{t\text{Bu}}$pyrr$_2$pyr)FeCl] (**5**) recorded in thf at 298 K. λ = 538 nm ε = 1210 M^{-1}. λ = 430 nm ε = 11300 M^{-1}. λ = 343 nm ε = 27200 M^{-1}.

8 Mössbauer Spectroscopy

8.1 Zero-field ^{57}Fe-Mössbauer spectrum of sample 1 of 5

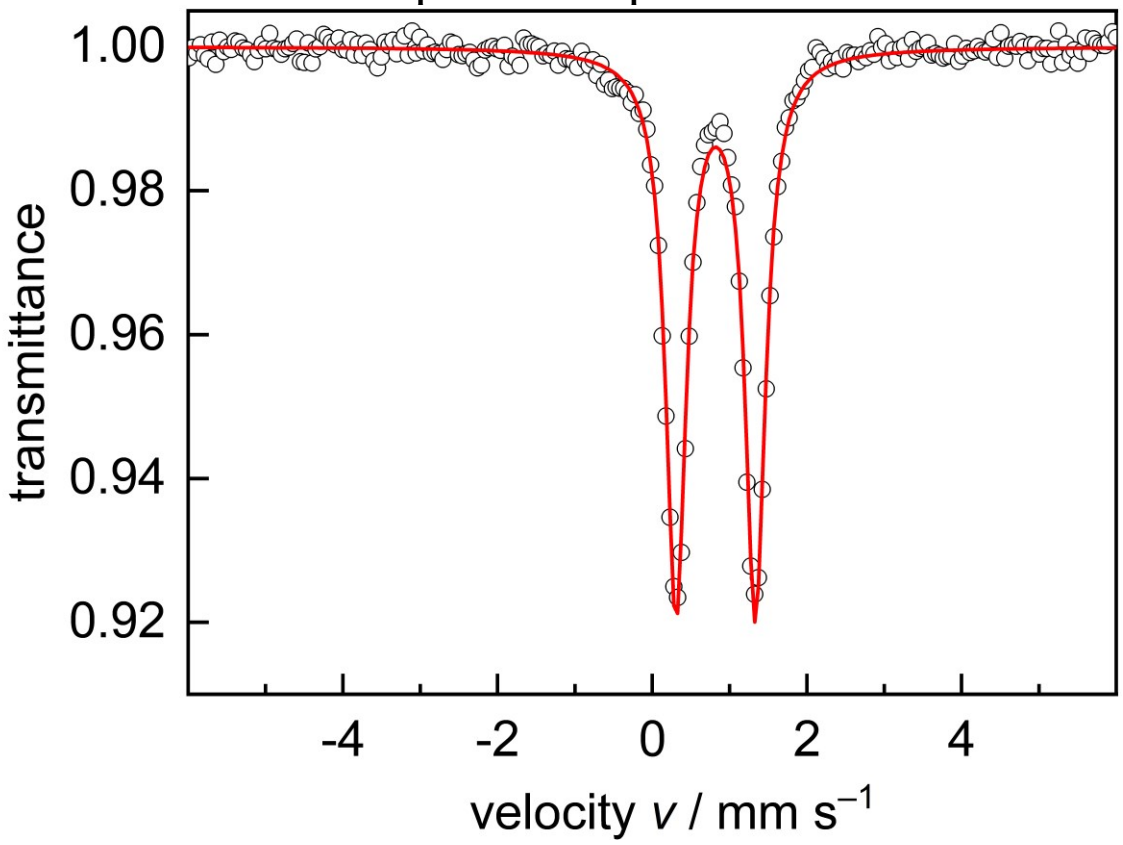

Figure S24. Zero-field ^{57}Fe-Mössbauer spectrum of sample 1 of [{K(18-crown-6)(thf)$_2$}($^{t\text{Bu}}$pyrr$_2$pyr)FeCl] (**5**), recorded in the solid state at 77 K. The red line represents the best overall fit obtained with the parameters given below.

^{57}Fe-Mössbauer (solid-state, 77 K): δ = 0.82 mm·s^{-1}, ΔE_Q = 1.02 mm·s^{-1}, Γ_{FWHM} = 0.32 mm·s^{-1}.

8.2 Zero-field ^{57}Fe-Mössbauer spectrum of sample 2 of 5

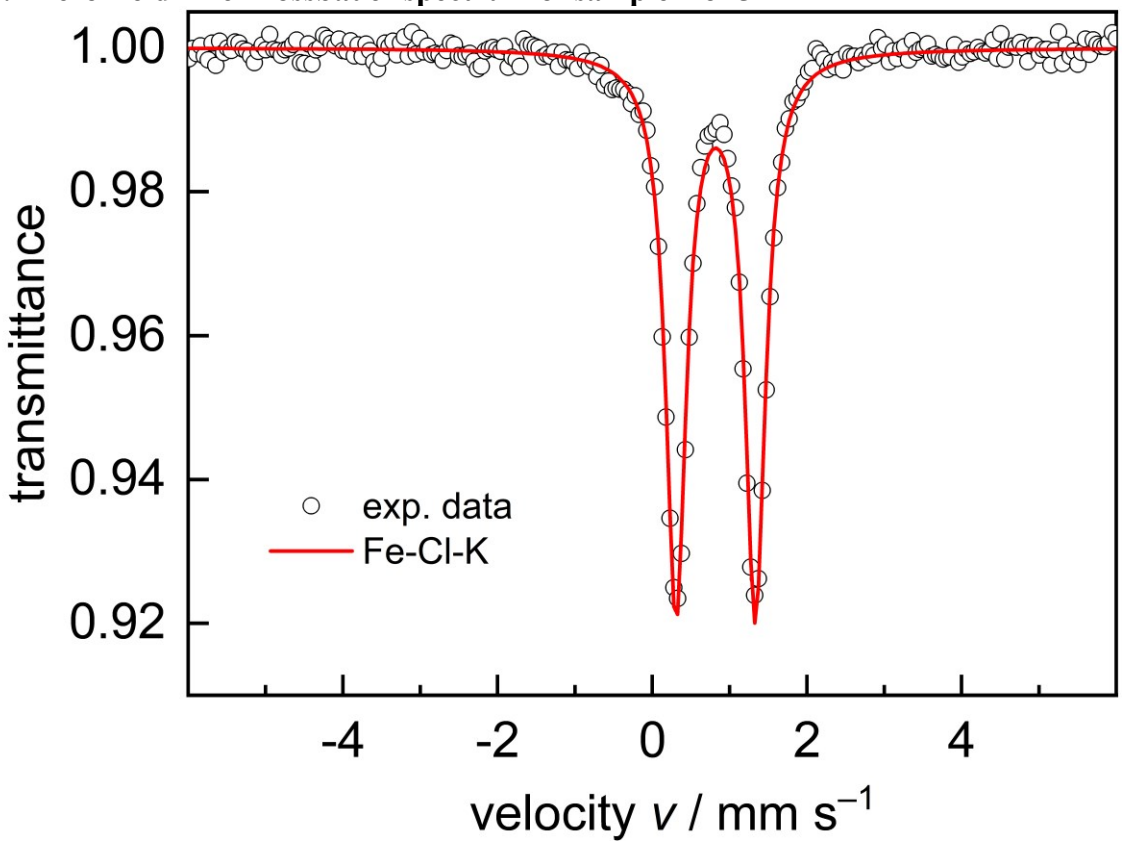

Figure S25. Zero-field ^{57}Fe-Mössbauer spectrum of sample 2 of [{K(18-crown-6)(thf)$_2$}($^{t\text{Bu}}$pyrr$_2$pyr)FeCl] (**5**), recorded in the solid state at 77 K. The red line represents the best overall fit obtained with the parameters given below.

^{57}Fe-Mössbauer (solid-state, 77 K): $\delta = 0.87$ mm·s^{-1}, $\Delta E_Q = 1.07$ mm·s^{-1}, $\Gamma_{FWHM} = 0.32$ mm·s^{-1}.

9 SQUID Magnetometry

9.1 Temperature-dependent SQUID DC field measurement of powdered sample 1 of 5

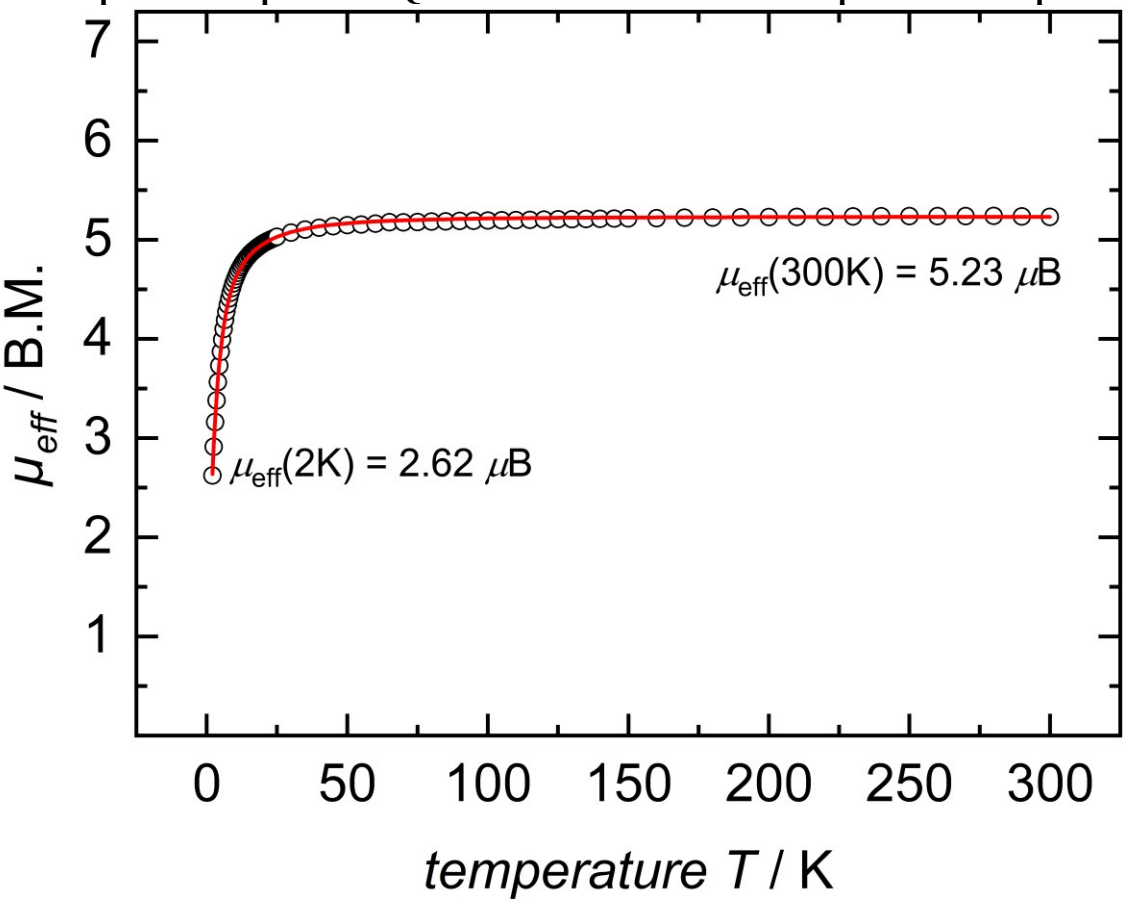

Figure S26. Temperature-dependent SQUID DC field measurement of powdered sample 1 of [{K(18-crown-6)(thf)$_2$}($^{t\text{Bu}}$pyrr$_2$pyr)FeCl] (**5**) recorded in a temperature range from 2 to 300 K with an applied magnetic field of 1 T. The solid line represents the best fit obtained with the parameters: S = 2, TIP = 1023 x 10^{-6} emu, |D| = 12 cm^{-1}, E/D = 0.14, g_{av} = 2.14.

9.2 Temperature-dependent SQUID DC field measurement of powdered sample 2 of 5

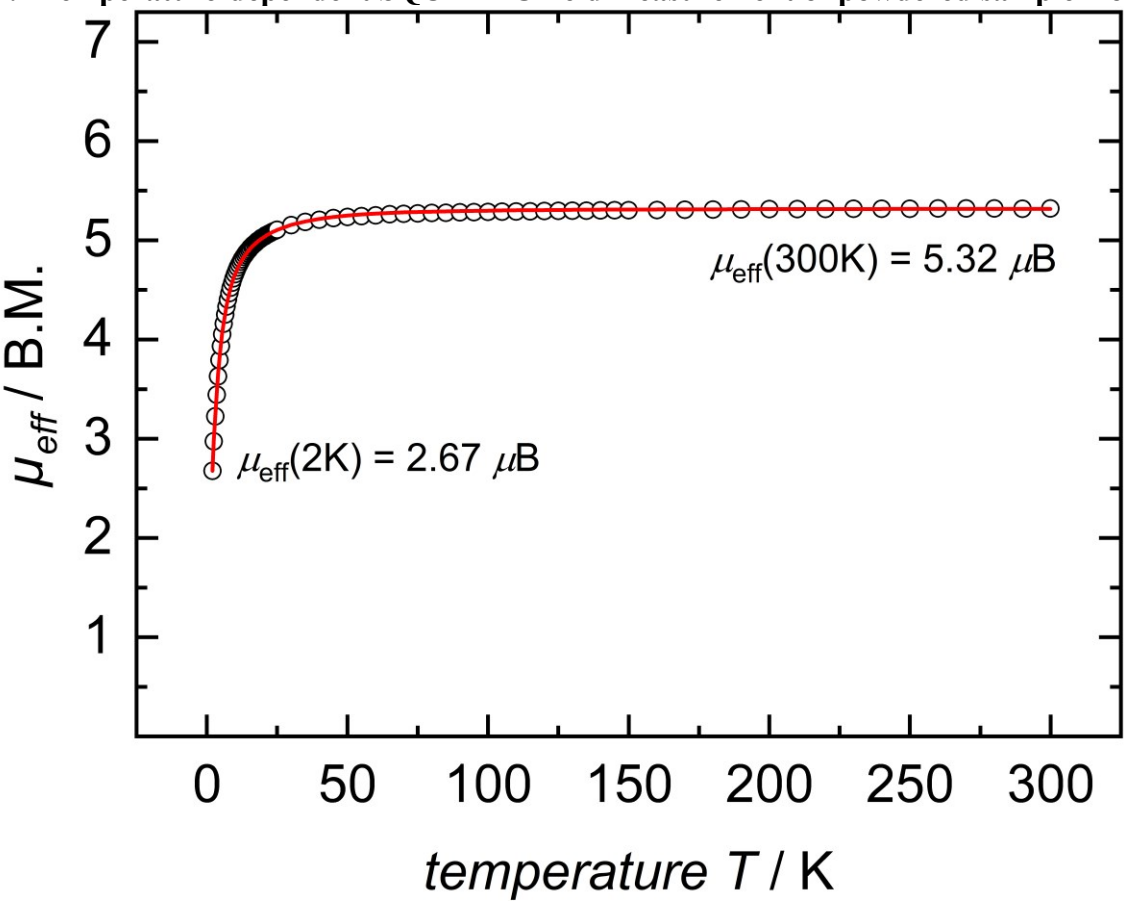

Figure S27. Temperature-dependent SQUID DC field measurement of powdered sample 2 of [{K(18-crown-6)(thf)$_2$}($^{t\text{Bu}}$pyrr$_2$pyr)FeCl] (**5**) recorded in a temperature range from 2 to 300 K with an applied magnetic field of 1 T. The solid line represents the best fit obtained with the parameters: S = 2, TIP = 3120 x 10^{-6} emu, |D| = 12 cm^{-1}, E/D = 0.14, g_{av} = 2.17.

9.3 VTVF SQUID DC field measurement of powdered sample 1 of 5

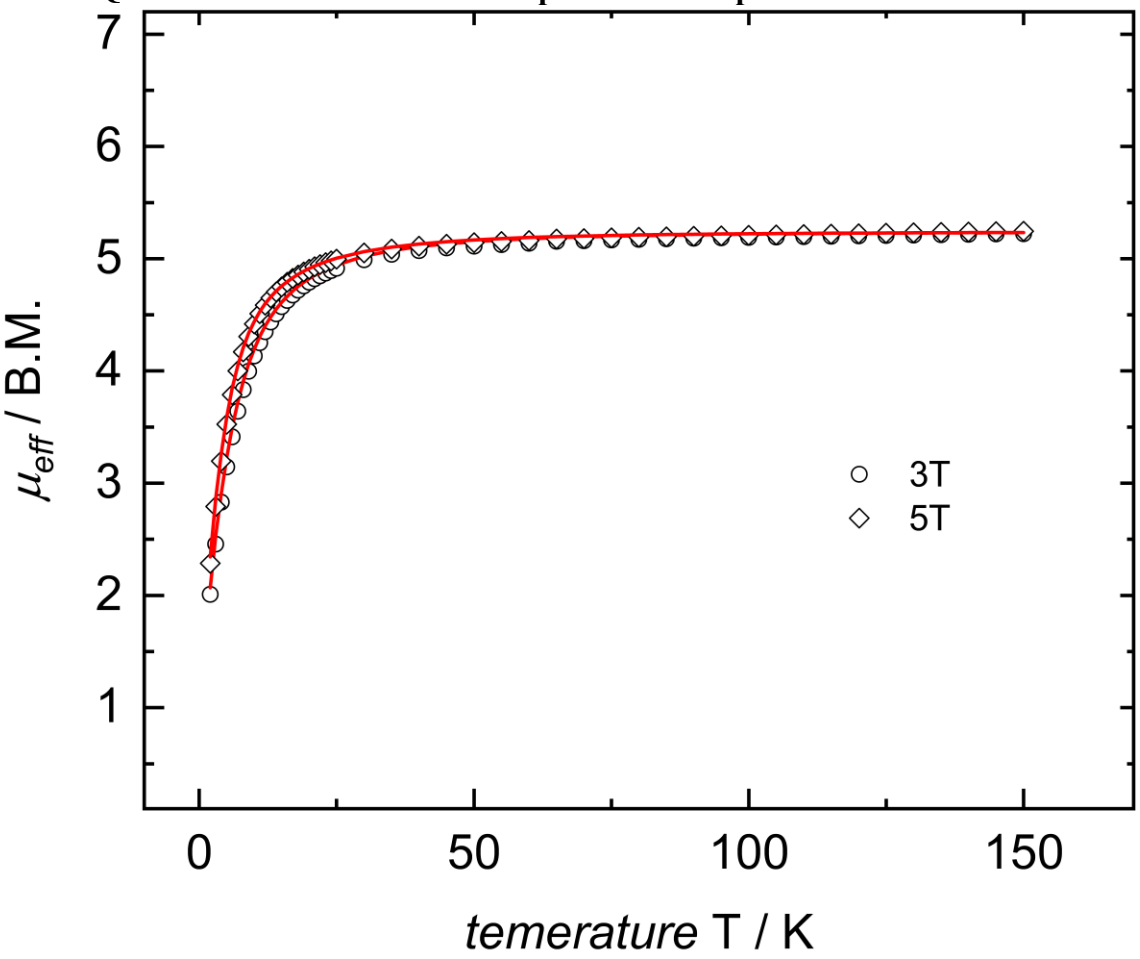

Figure S27. Temperature-dependent SQUID DC field VTVF measurement of powdered sample 1 of [{K(18-crown-6)(thf)$_2$}($^{t\text{Bu}}$pyrr$_2$pyr)FeCl] (**5**), recorded in a temperature range from 2 to 150 K with an applied magnetic field of 3 T and 5 T. The solid line represents the best fit obtained with the parameters: S = 2, TIP = 1023 x 10^{-6} emu, |D| = 12 cm^{-1}, E/D = 0.14, g_{av} = 2.14.

9.4 VTVF SQUID DC field measurement of powdered sample 2 of 5

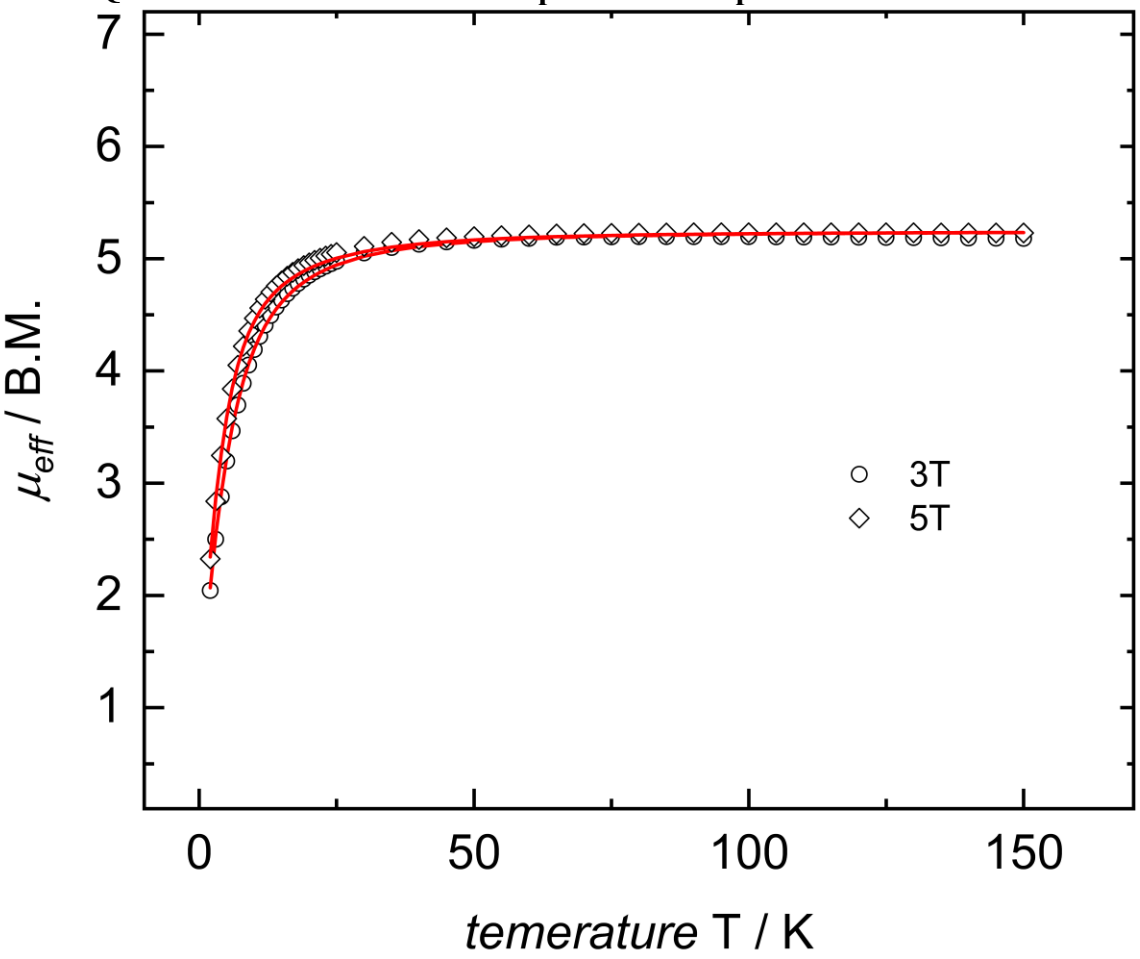

Figure S28. Temperature-dependent SQUID DC field VTVF measurement of powdered sample 1 of [{K(18-crown-6)(thf)$_2$}($^{t\text{Bu}}$pyrr$_2$pyr)FeCl] (**5**), recorded in a temperature range from 2 to 150 K with an applied magnetic field of 3 T and 5 T. S = 2, TIP = 3120 x 10^{-6} emu, |D| = 12 cm^{-1}, E/D = 0.14, g_{av} = 2.17.

9.5 Combined SQUID DC field measurements of powdered samples 1 and 2 of 5

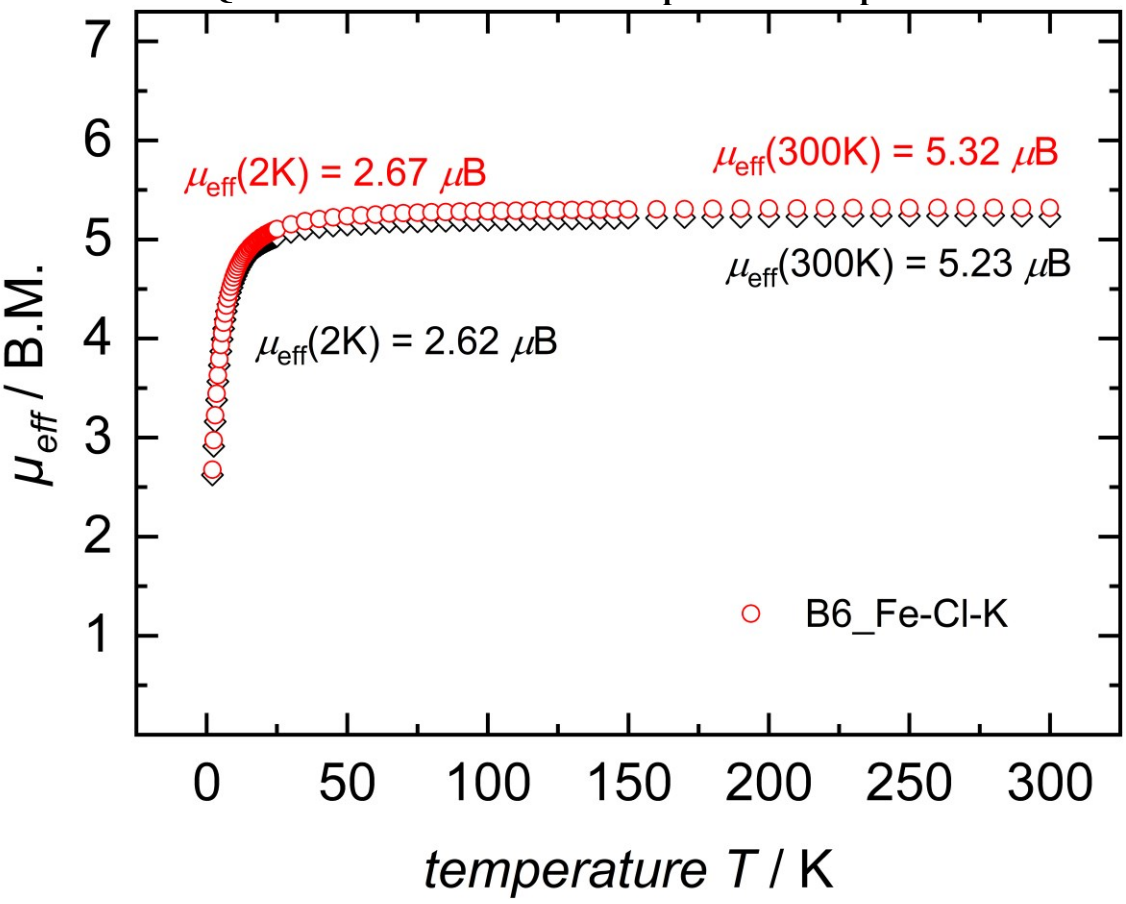

Figure S29. Temperature-dependent SQUID DC field measurements of two powdered samples of [{K(18-crown-6)(thf)$_2$}($^{t\text{Bu}}$pyrr$_2$pyr)FeCl] (**5**) (sample 1 black diamonds, sample 2 red circles) recorded in a temperature range from 2 to 300 K with an applied magnetic field of 1 T.

10 X-Ray Crystallography

10.1 *sc*-XRD structure of 2

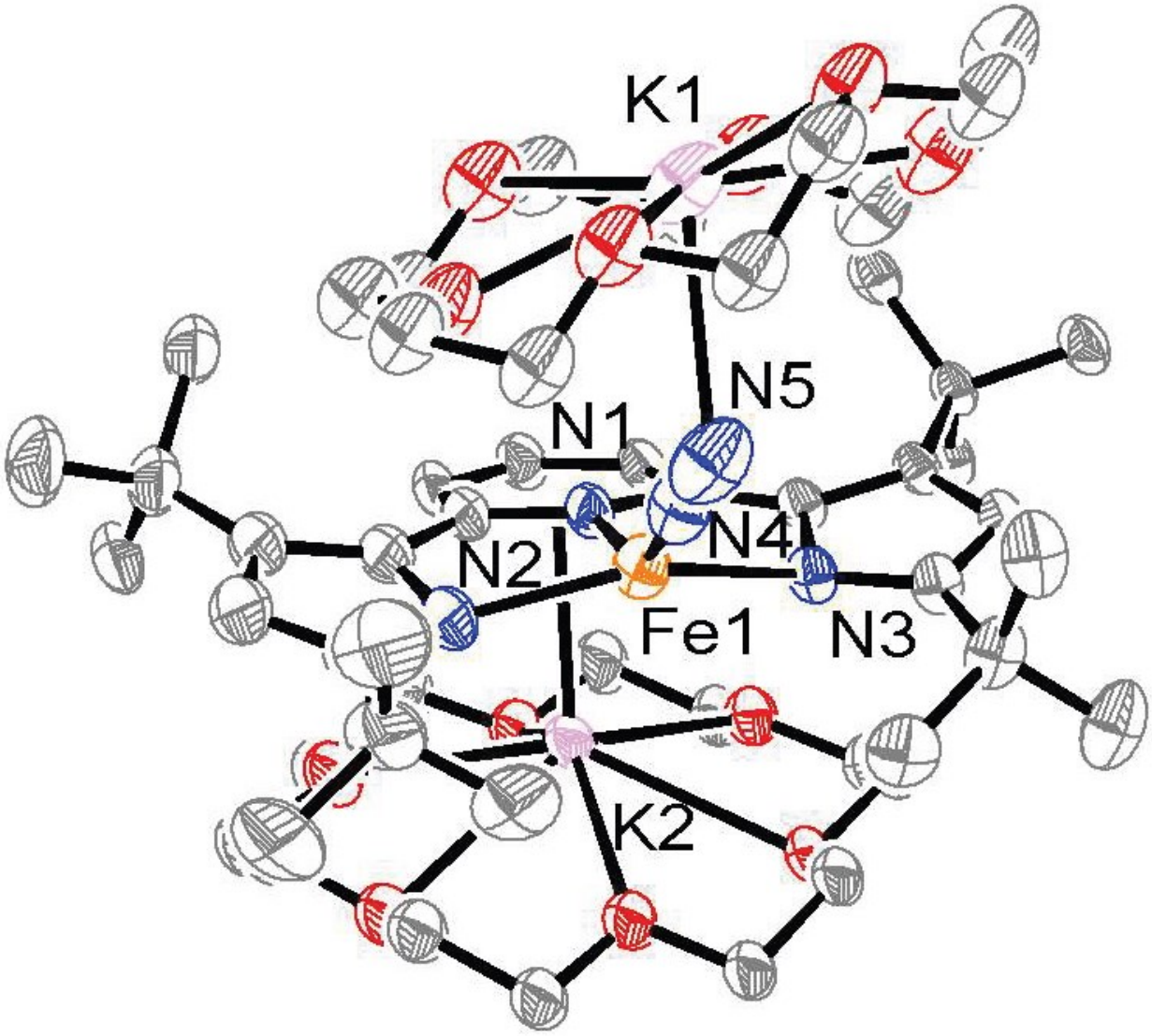

Figure S30. *sc*-XRD structure of **2** at 50% probability. Solvent molecules and H atoms have been omitted for clarity.

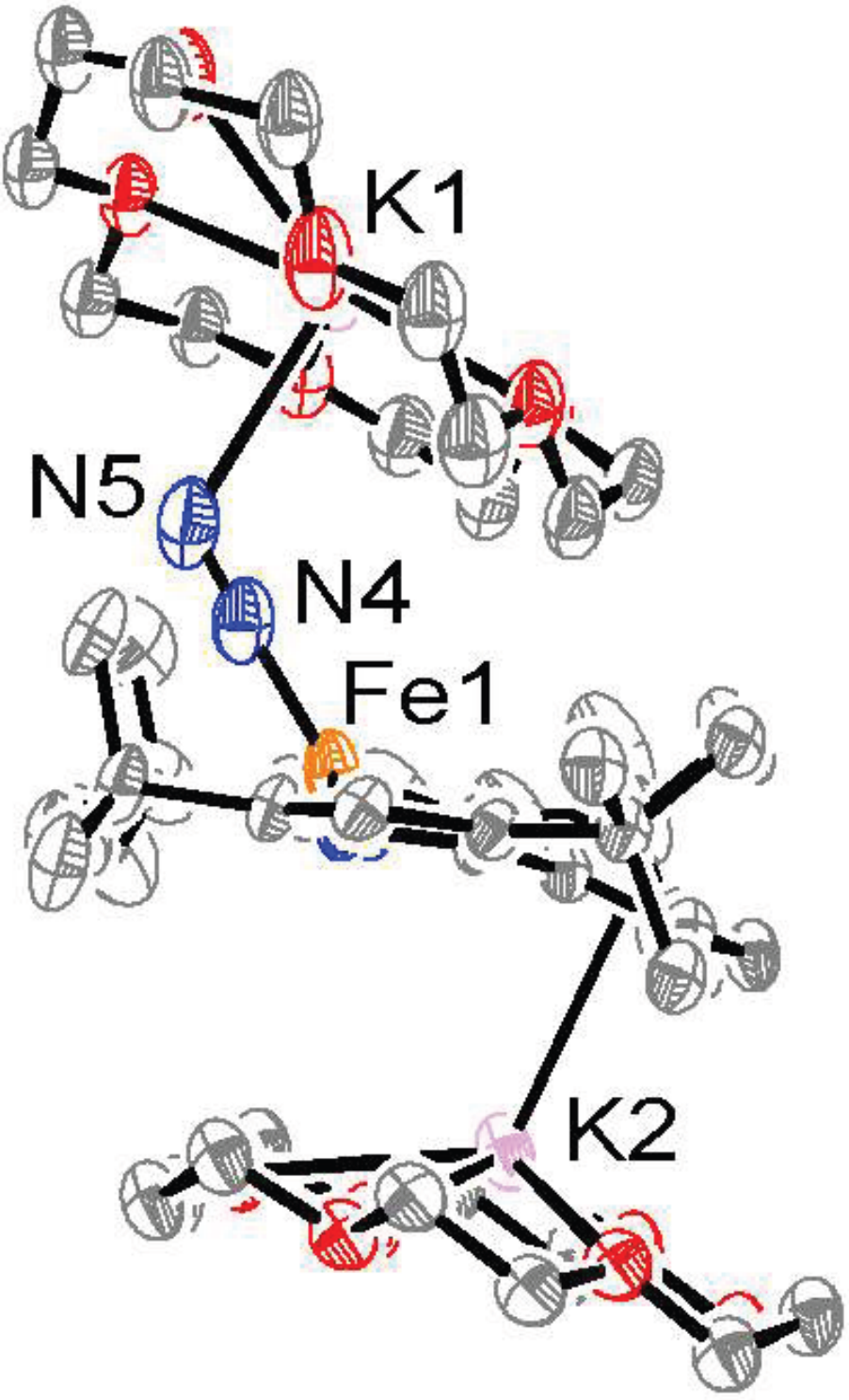

Figure S31. *sc*-XRD structure of **2** at 50% probability. Solvent molecules and H atoms have been omitted for clarity.

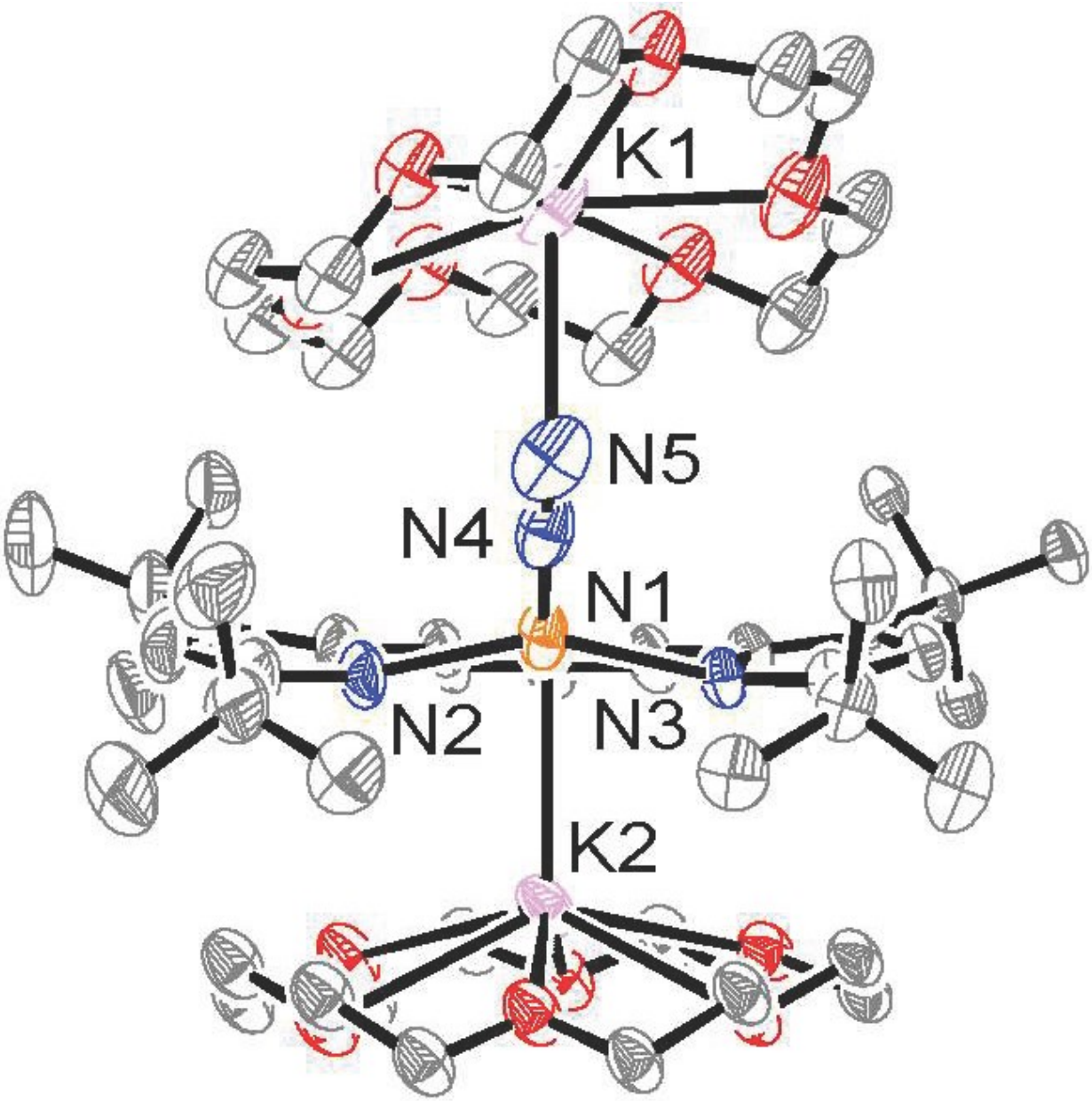

Figure S32. *sc*-XRD structure of **2** at 50% probability. Solvent molecules and H atoms have been omitted for clarity.

10.2 *sc*-XRD structure of 3

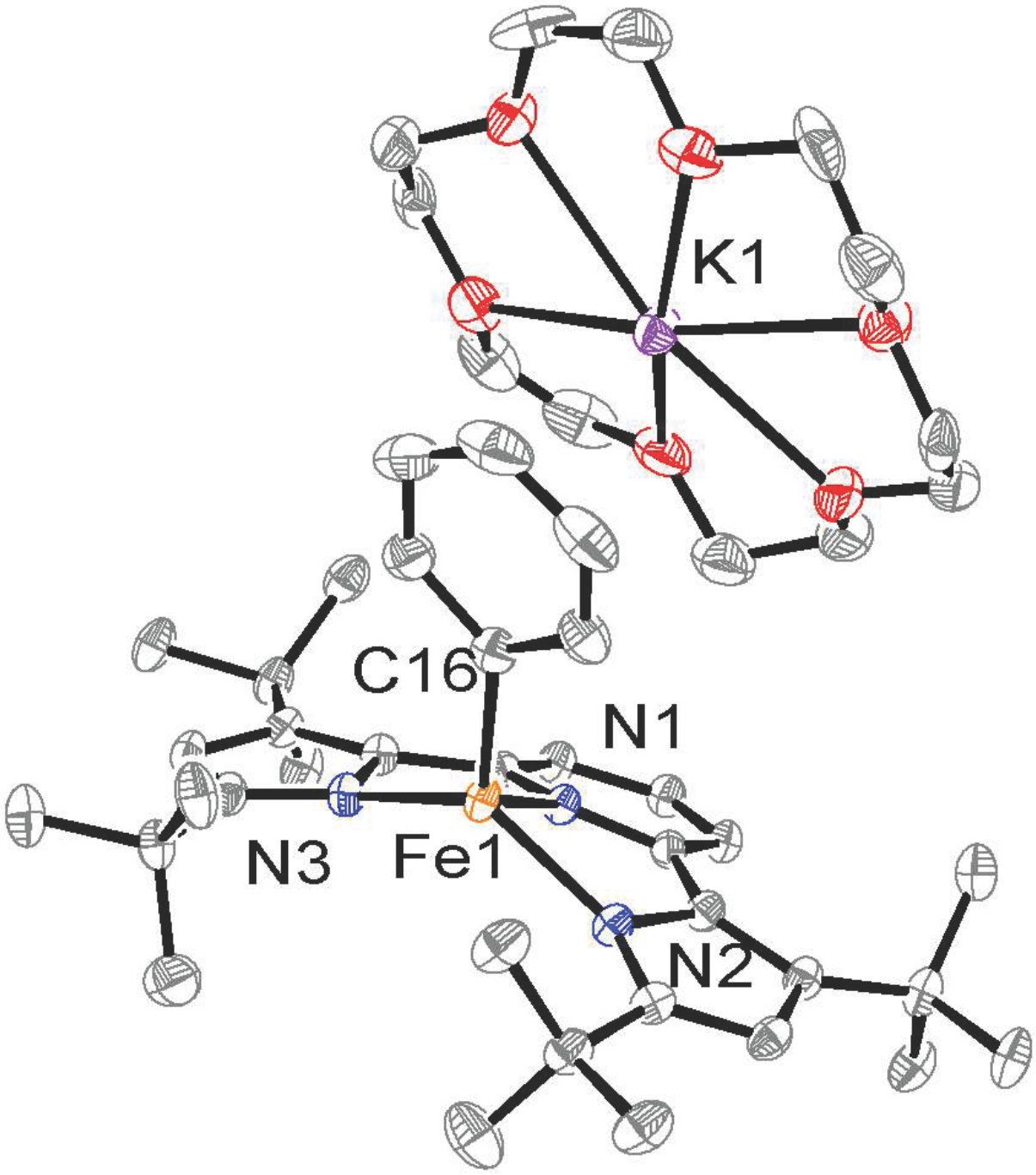

Figure S33. *sc*-XRD structure of **3** at 50% probability. Solvent molecules and H atoms have been omitted for clarity.

10.3 *sc*-XRD structure of 4

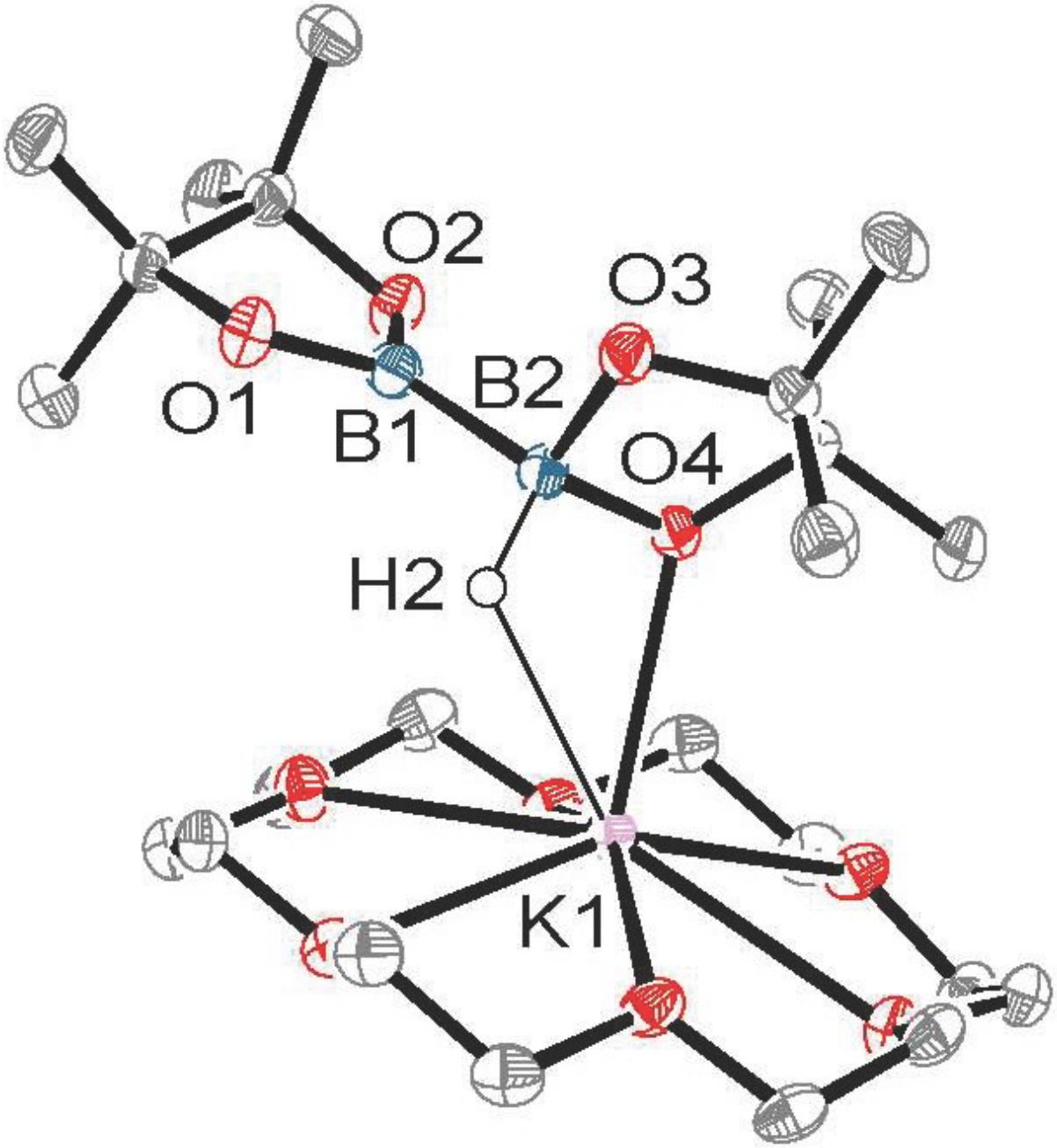

Figure S34. *sc*-XRD structure of **4** at 50% probability. Solvent molecules and most H atoms have been omitted for clarity.

10.4 *sc*-XRD structure of 5

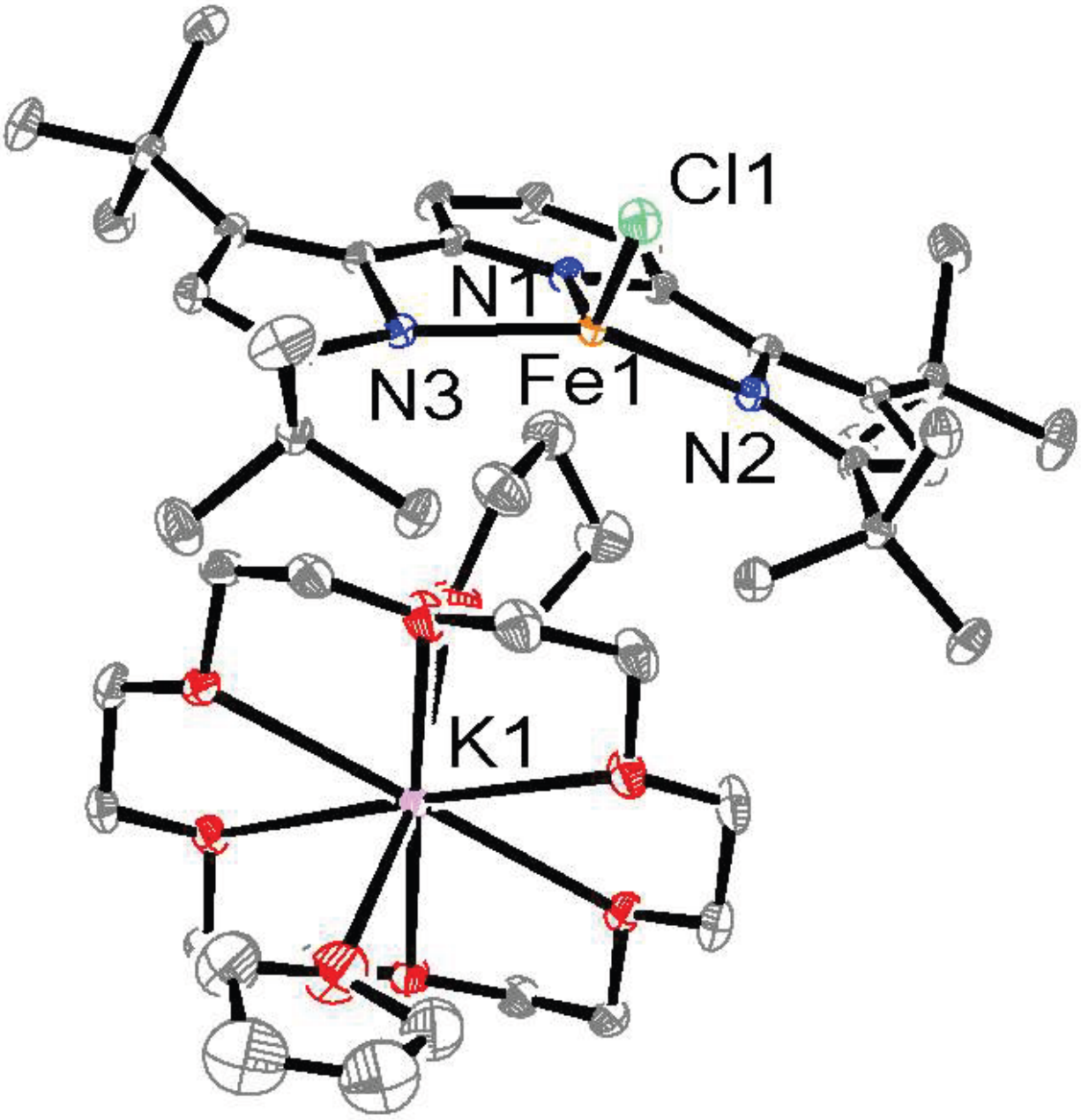

Figure S35. *sc*-XRD structure of **5** at 50% probability. Some solvent molecules and H atoms have been omitted for clarity.

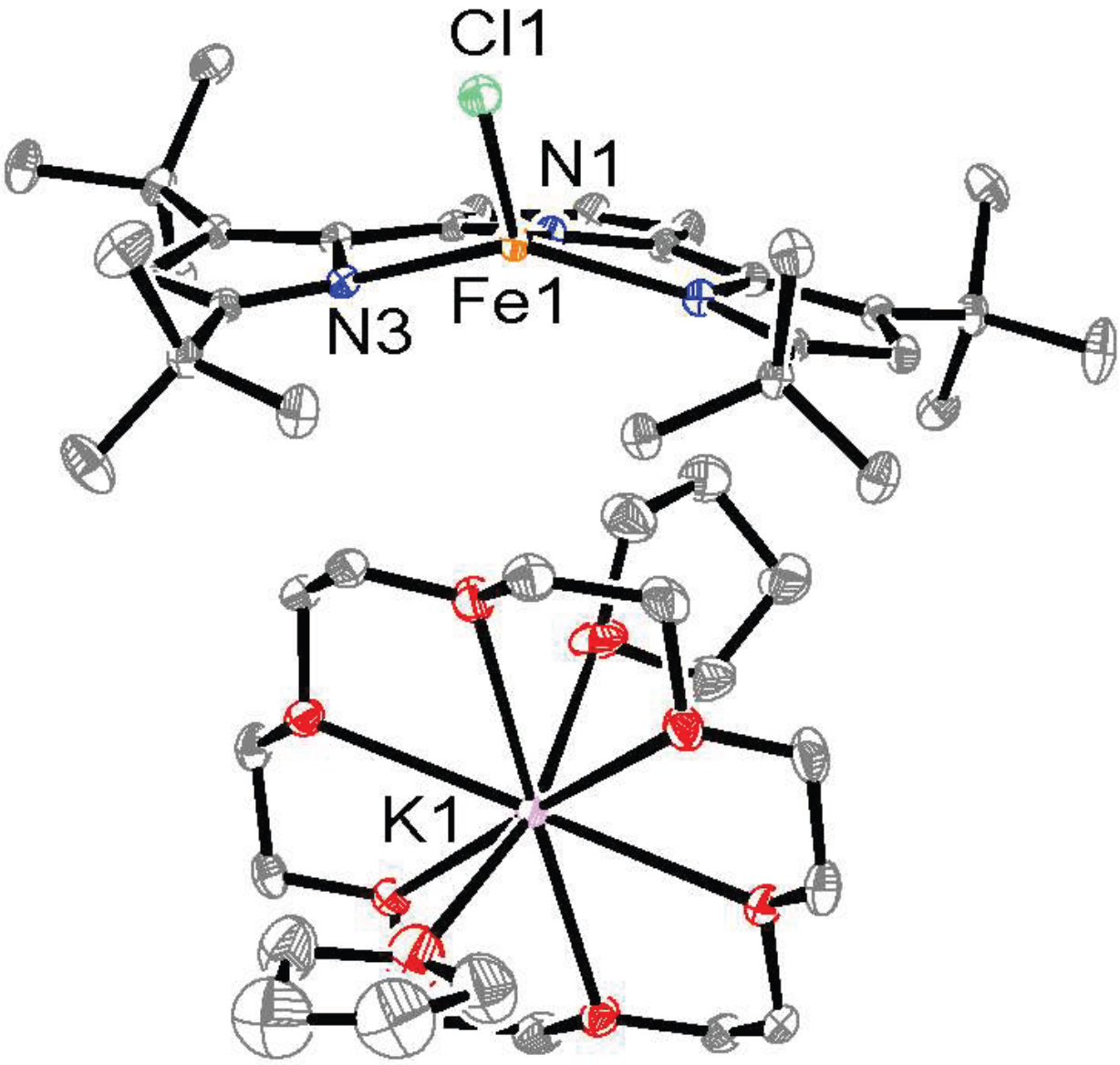

Figure S36. *sc*-XRD structure of **5** at 50% probability. Some solvent molecules and H atoms have been omitted for clarity.

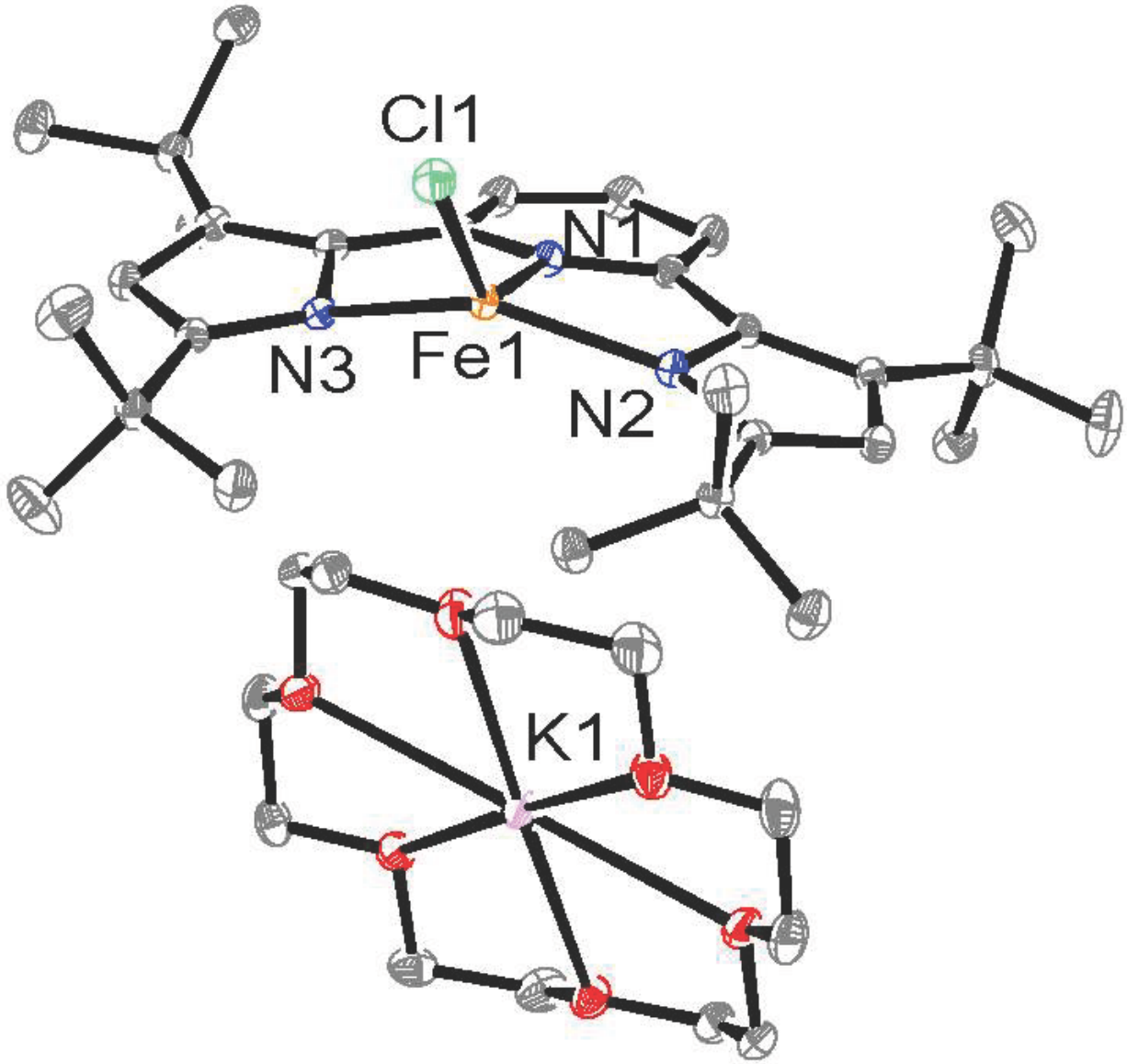

Figure S37. *sc*-XRD structure of **5** at 50% probability. Solvent molecules and H atoms have been omitted for clarity.

10.5 Table of crystallographic information

Table S1. Crystallographic Information for **2**, **3**, **4**, and **5**.

	2	**3**	**4**	**5**
Empirical formula	$C_{53}H_{89}FeK_2N_5O_{12}$	$C_{53}H_{76}FeKN_3O_6$	$C_{24}H_{49}B_2KO_{10}$	$C_{53}H_{89}ClFeKN_3O_9$
Formula weight	1122.34	946.11	558.35	1042.67
Temperature/K	100	100	100	100
Crystal system	monoclinic	monoclinic	monoclinic	monoclinic
Space group	$P2_1/c$	$P2_1/m$	$P2_1/n$	$P2_1/n$
Cell Constants				
a	21.8155(4)Å	9.6800(6)Å	10.16110(10)Å	14.8545(3)Å
b	9.8873(2)Å	23.1914(11)Å	19.4480(2)Å	23.4401(4)Å
c	27.5274(5)Å	12.1542(9)Å	15.5969(2)Å	16.8987(3)Å
α	90°	90°	90°	90°
β	90.332(2)°	108.201(7)°	95.9250(10)°	103.340(2)°
γ	90°	90°	90°	90°
Volume	5937.46(19)Å^3	2592.0(3)Å^3	3065.69(6)Å^3	5725.21(19)Å^3
Z	4	2	4	4
d_{calc}	1.256 g/cm^3	1.212 g/cm^3	1.210 g/cm^3	1.210 g/cm^3
μ	0.454 mm^{-1}	0.421 mm^{-1}	0.221 mm^{-1}	0.436 mm^{-1}
F(000)	2408.0	1016.0	1208.0	2248.0
Crystal size, mm	0.38 × 0.27 × 0.27	0.26 × 0.07 × 0.02	0.59 × 0.48 × 0.37	0.32 × 0.16 × 0.13
2θ range for data collection	6.29 - 50.69°	3.94 - 56.666°	6.55 - 56.378°	4.16 - 56.566°
Index ranges	$-26 \le h \le 26$, $-11 \le k \le 11$, $-33 \le l \le 33$	$-12 \le h \le 12$, $-30 \le k \le 30$, $-16 \le l \le 16$	$-13 \le h \le 13$, $-25 \le k \le 25$, $-20 \le l \le 20$	$-19 \le h \le 19$, $-31 \le k \le 31$, $-22 \le l \le 22$
Reflections collected	162380	77745	115890	175002
Independent reflections	10842[R(int) = 0.0789]	16553[R(int) = 0.100]	7378[R(int) = 0.0417]	14209[R(int) = 0.0461]
Refinement Method	Full matrix least squares	Full matrix least squares	Full matrix least squares	Full matrix least squares
Data/restraints/parameters	10842/1128/996	16553/125/386	7378/0/349	14209/138/688
Goodness-of-fit on F^2	1.068	0.917	1.031	1.028
Final R indexes [I>=2σ (I)]	$R_1 = 0.0814$, $wR_2 = 0.1873$	$R_1 = 0.0596$, $wR_2 = 0.1309$	$R_1 = 0.0347$, $wR_2 = 0.0828$	$R_1 = 0.0322$, $wR_2 = 0.0773$
Final R indexes [all data]	$R_1 = 0.0958$, $wR_2 = 0.1956$	$R_1 = 0.1009$, $wR_2 = 0.1462$	$R_1 = 0.0419$, $wR_2 = 0.0857$	$R_1 = 0.0395$, $wR_2 = 0.0801$
Largest diff. peak/hole	0.82/-0.64 eÅ^{-3}	0.58/-0.37 eÅ^{-3}	0.55/-0.22 eÅ^{-3}	0.63/-0.35 eÅ^{-3}

11 References

1 N. Komine, R. W. Buell, C.-H. Chen, A. K. Hui, M. Pink and K. G. Caulton, *Inorg. Chem.*, 2014, **53**, 1361–1369.

2 D. L. J. Broere, I. Čorić, A. Brosnahan and P. L. Holland, *Inorg. Chem.*, 2017, **56**, 3140–3143.

3 K. Searles, S. Fortier, M. M. Khusniyarov, P. J. Carroll, J. Sutter, K. Meyer, D. J. Mindiola and K. G. Caulton, *Angew. Chem., Int. Ed.*, 2014, **53**, 14139–14143.

4 D. Sorsche, M. E. Miehlich, K. Searles, G. Gouget, E. M. Zolnhofer, S. Fortier, C.-H. Chen, M. Gau, P. J. Carroll, C. B. Murray, K. G. Caulton, M. M. Khusniyarov, K. Meyer and D. J. Mindiola, *J. Am. Chem. Soc.*, 2020, **142**, 8147–8159.

5 E. M. Schubert, *J. Chem. Educ.*, 1992, **69**, 62.

6 G. A. Bain and J. F. Berry, *J. Chem. Educ.*, 2008, **85**, 532.

7 E. Bill, 2019. Mössbauer Program mcal

8 E. Bill, 2019. SQUID Program julX2

9 Z. Zheng, O. S. Trofymchuk, T. Kurogi, E. Varela, D. J. Mindiola and P. J. Walsh, *Adv. Synth. Catal.*, 2020, **362**, 659–666.

10 S. Kharbanda and J. D. I. I. I. Weaver, *J. Org. Chem.*, 2023, **88**, 6434–6444.

11 D.-G. Yu and Z.-J. Shi, *Angew. Chem., Int. Ed.*, 2011, **50**, 7097–7100.

12 F. P. Gabbaï, P. J. Chirik, D. E. Fogg, K. Meyer, D. J. Mindiola, L. L. Schafer and S.-L. You, *Organometallics*, 2016, **35**, 3255–3256.

13 A. Katsnelson, *ACS Cent Sci*, 2022, **8**, 1569–1572.

14 S. Proctor, S. Lovera, A. Tomich and V. Lavallo, *ACS Cent. Sci.*, 2022, **8**, 874–876.

15 R. E. H. Kuveke, L. Barwise, Y. van Ingen, K. Vashisth, N. Roberts, S. S. Chitnis, J. L. Dutton, C. D. Martin and R. L. Melen, *ACS Cent. Sci.*, 2022, **8**, 855–863.

16 W. Kandioller, J. Theiner, B. K. Keppler and C. R. Kowol, *Inorg. Chem. Front.*, 2022, **9**, 412–416.